REVIEWS OF GEOPHYSICS AND SPACE PHYSICS, VOL. 18, NO. 4, PAGES 862–886, NOVEMBER 1980

Thermodynamics and Lattice Vibrations of Minerals: 4. Application to Chain and Sheet Silicates and Orthosilicates

SUSAN WERNER KIEFFER

U.S. Geological Survey, Flagstaff, Arizona 86001

This paper is the fourth in a series relating the lattice vibrational properties to the thermodynamic properties of minerals. The temperature dependence of the harmonic lattice heat capacity is calculated from a model which uses only elastic, crystallographic, and spectroscopic data for the following minerals: calcite, zircon, forsterite, grossular, pyrope, almandine, spessartine, andradite, kyanite, andalusite, sillimanite, clinoenstatite, orthoenstatite, jadeite, diopside, tremolite, talc, and muscovite. The heat capacities of these minerals reflect structural and compositional differences. The 'excess' entropy of pyrope—compared with that of grossular—is shown to arise from low-frequency optic modes of vibration. The entropy differences between kyanite, andalusite, and sillimanite are well reproduced by the model, although the absolute values calculated are systematically about 3% high. Model values of the heat capacity and entropy are compared with experimental values at 298.15, 700, and 1000°K for the 32 minerals included in papers 1–4 of this series. The average deviation of the entropies at 298°K from well-determined calorimetric values is ± 1.5%. A method is given for obtaining greater accuracy in the model thermodynamic functions by fitting one parameter to experimental data when partial calorimetric data (such as the heat capacity at a single temperature in the range 50–100°K) are available; such a method should permit accurate extrapolation of calorimetric data beyond the range of experiment.

CONTENTS

1. INTRODUCTION

This is paper 4 of a series of papers in which a generalized model of lattice vibrations for complex minerals is developed and applied to give the temperature dependence of the harmonic contribution to the thermodynamic functions for 32 minerals (see the papers by *Kieffer* [1979*a*, *b*, *c*], referred to as papers 1, 2, and 3). In paper 3 of this series the model was applied to some simple minerals and framework silicates; in this paper it is applied to some chain and sheet silicates and orthosilicates and to calcite. The minerals examined were selected for detailed discussion to illustrate the strong relationships between mineral composition and structure and elastic, spectral, and thermodynamic properties. At the risk of wearying the reader with details these parameters are discussed for each mineral rather than listed in a summary table, because the author feels it necessary to emphasize the interrelationships amongst the various physical properties influencing the thermodynamic properties. The study of the temperature dependence of the thermodynamic functions presented in papers 1–4 is concluded in this paper. The thermodynamic quantities discussed here are the heat capacity at constant volume, C_V^*, and the entropy S^*. (The asterisk indicates quantities normalized to the monatomic equivalent, that is, quantities per mole divided by the number of atoms per formula unit; strictly speaking, these quantities should be referred to as per mean atomic weight, but for brevity they are denoted as per mole in the text. These molar quantities should not be confused with the standard state functions conventionally denoted by the superscript zero.) The tabulated values are the harmonic contribution to the thermodynamic functions; estimates of the anharmonic correction which must be added to C_V^* for comparison with measured values of C_P^* and to the 'harmonic' entropy

$$\int_0^{T_f} (C_V^*/T)\, dT$$

for comparison with the measured total entropy

$$\int_0^{T_f} (C_P^*/T)\, dT$$

are given. In paper 5 of this series [*Kieffer*, 1980] the pressure dependence of the functions will be estimated from the model, and applications to several problems of phase equilibria and isotopic fractionation will be given.

The reader is referred to paper 3 for a description of the model and notation used and to papers 1 and 2 for many of the elastic and spectral parameters used for individual minerals.

2. THE MODEL

The model developed in papers 1–3 is shown schematically in Figures 1*a* and 1*b*. The vibrational unit of a crystal is taken

Paper number 80R1044.

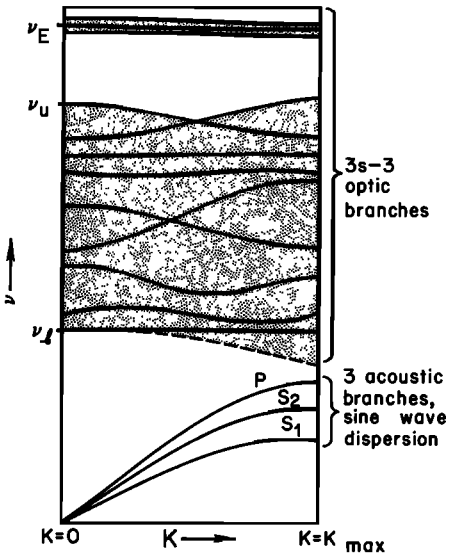

Fig. 1*a*. Schematic dispersion curves for the model given in paper 3. There are $3s$ branches, corresponding to the $3s$ degrees of freedom of the Bravais unit cell. Three are acoustic branches (two shear branches, S_1 and S_2, and one longitudinal branch, P) which are assumed to obey a sine wave dispersion relation. There are $3s - 3$ optic modes, which may follow complex dispersion relations indicated schematically within the shaded zone. These relations may also vary with direction of the wave vector **K** in the Brillouin zone. In the model the optic modes are treated as follows: if some fractions q_1, q_2, ··· of these lie at isolated high frequencies, they are represented by a single Einstein oscillator at ν_{E_1}, ν_{E_2}, ···; the remaining modes are assumed to be distributed uniformly in a continuum between ν_l and ν_u.

as the Bravais or primitive unit cell in accordance with Bloch's theorem [*Ziman*, 1972, p. 17]. If the primitive unit cell contains a number of atoms denoted by s, then $3s$ total degrees of freedom are associated with the unit cell. Each mode of vibration appears as a separate branch on a dispersion plot (a plot of wave vector **K** versus frequency ν) such as that shown in Figure 1*a*. The dispersion relations can be different in each direction of the crystal because of anisotropy.

Of the $3s$ degrees of freedom, only three are acoustic modes, which, by definition, approach zero frequency as the wave vector **K** approaches zero. Two shear modes (S_1 and S_2) and one longitudinal (P) mode are included in the model and are characterized by acoustic velocities as described in paper 1. A simple sine wave dispersion of the modes toward the edge of the Brillouin zone is assumed, in accordance with monatomic chain theory and the general tendency for measured curves to flatten toward the zone boundary. Note that because most minerals contain a large number of atoms in a unit cell, say, more than 10 atoms, acoustic modes constitute only a small fraction ($1/s$) of the total modes.

The remaining ($3s - 3$) modes are optic modes which span a broad range of frequencies, both at the zone center and throughout the Brillouin zone. An estimate of the range of the optic modes can be obtained from far- and mid-infrared spectroscopy, but for most minerals we have no information about the behavior of the dispersion curves and therefore about the range of frequencies away from the zone center. Because the thermodynamic functions are sensitive to details of the vibrational spectrum only at low frequencies, it is only at the lowest frequencies that a correct estimate of the dispersion relations appears to be essential for thermodynamic calculations. I assume that the frequency of the lowest optic mode varies (as in the monatomic chain model) inversely with a characteristic mass ratio across the Brillouin zone (equation (19*b*) in paper 3). Because the lowest-frequency deformations are usually cation-oxygen deformations, I use masses of the heavy (or weakly linked) cation (denoted as m_1) and of oxygen (denoted as m_2) for the required ratio (these are given in Table 6 of paper 2).

The optic modes are assumed to follow the simplest possible frequency distribution $g(\nu)$: they are assumed to be distributed uniformly between a lower cutoff frequency ν_l and an upper cutoff frequency ν_u, both of which can be specified from spectroscopic (infrared, Raman, or inelastic neutron scattering) data, with the specified lower cutoff frequency corrected for dispersion across the Brillouin zone as discussed above. The height of the optical continuum is determined from normalization of the total number of optical modes to ($3s - 3$) for the primitive unit cell.

Where some of the modes (such as silicon-oxygen stretching modes, hydroxyl stretching modes, or carbonate bending or stretching modes) are isolated at high frequencies from the lower-frequency bending modes or weaker stretching modes of other cation-oxygen bonds, it is possible and desirable (for accuracy) to include more information in the specification of the distribution of the optic modes. A scheme was given in paper 2 for enumerating these modes (which might loosely be referred to as 'intramolecular'); this scheme is discussed in further detail in this paper. Such modes are then placed in one or more Einstein oscillators, designated as ν_{E_1}, ν_{E_2}, ···. The fraction of the total modes associated with each oscillator is designated as q_1, q_2, ···.

In summary, the lattice frequency distribution is approximated in the model as follows (Figure 1*b*): the whole central part of the spectrum, which corresponds roughly to far- and mid-infrared spectral frequencies, is represented by a uniform density of states called the 'optical continuum.' Any isolated modes which can be enumerated are represented as separate Einstein oscillators. The three acoustic branches are obtained by integrating the assumed acoustic dispersion curves shown in Figure 1*a*. The assumed frequency distribution is the sum of these three different parts, as shown in Figure 1*b*, and it is used in the equations of paper 1, Table 1, to generate the harmonic thermodynamic functions.

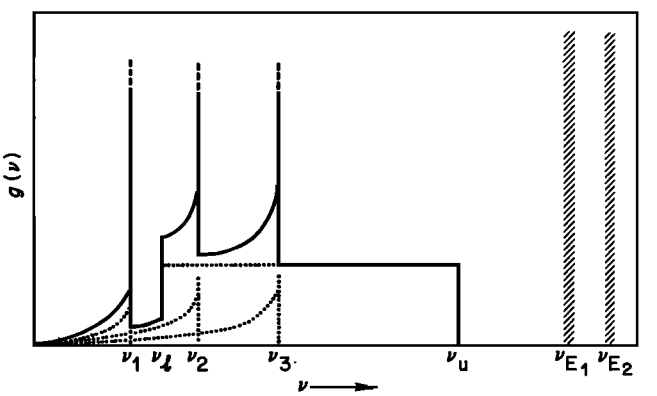

Fig. 1*b*. Schematic frequency distribution used in the model. The three acoustic branches are shown separately as the dotted curves rising from ν_1, ν_2, and ν_3. The optic continuum is the flat distribution between ν_l and ν_u. The total spectrum (sum of acoustic and optic branches) is shown by the solid curve. Separate Einstein oscillators are shown at ν_{E_1} and ν_{E_2}; for a more accurate model (such as is required for the isotopic fractionation calculations discussed in paper 5) these could be spread into bands.

TABLE 1. Summary of Recommended Model Parameters for all Minerals Considered in Papers 1–4

Mineral	z (Primitive Cell)	S	V_L, 10^{-24} cm^{-3}	ρ g cm^{-3}	u_1, km s^{-1}	u_2, km s^{-1}	$v_{VRH,S}$ km s^{-1}	$v_{VRH,P}$ km s^{-1}	v_m, km s^{-1}	θ_{el}, °K	w_1, cm^{-1}	w_2, cm^{-1}	w_3, cm^{-1}	$w_l(0)$, cm^{-1}	$w_l(K_{max})$, cm^{-1}	w_w, cm^{-1}	m_1/m_2	w_{E_1}, cm^{-1}	q_1	w_{E_2}, cm^{-1}	q_2	w_{E_3}, cm^{-1}	q_3	w_{E_4}, cm^{-1}	q_4
Halite	1	2	44.8	2.16	2.50	2.74	2.61	4.56	2.90	306	93	102	170	173	135	265	35/23								
Periclase	1	2	18.9	3.58	5.83	6.30	6.05	9.71	6.66	942	290	313	482	390	303	730	24/16								
Brucite	1	5	63.7	2.37	4.25	4.25	4.25	7.36	4.72	697	141	141	244	280	198	725	58/58							3670	0.133
Corundum	2	10	84.9	3.99	6.12	6.59	6.41	10.85	7.03	1026	184	198	327	378	300	751	27/16								
Spinel 1	2	14	131.9	3.58	5.31	6.00	5.62	9.82	6.24	879	138	156	255	311[a]	246	600	27/16	700	0.19						
Spinel 2	2	14	131.9	3.58	5.31	6.00	5.62	9.82	6.24	879	138	156	255	311[a]	246	750	27/16								
α-Quartz	3	9	113.0	2.65	3.76	4.46	4.05	6.05	4.42	567	103	122	165	128	90	809	16/16	1200	0.074	1162	0.037	1117	0.074	1080	0.037[b]
α-Cristobalite	4	12	170.9	2.32	3.56	4.23	3.84	6.17	4.23	519	85	101	147	118	83	804	16/16	1200	0.074	1162	0.037	1117	0.074	1080	0.037[b]
Vitreous silica CRN	(see text)	3×10^5	10^6	2.20	3.74	3.74	3.74	5.50	4.08	491	5	5	7	7	5	804	16/16	1200	0.074	1162	0.037	1117	0.074	1080	0.037[b]
Vitreous silica PD	(see text)	3375	5×10^4	2.20	3.74	3.74	3.74	5.50	4.08	491	13	13	20	19	13	804	16/16	1200	0.074	1162	0.037	1117	0.074	1080	0.037[b]
Coesite 1	8	24	274.0	2.92	4.17	5.24	4.59	8.19	5.10	676	85	107	167	121	86	683	16/16	1200	0.074	1162	0.037	1117	0.074	1080	0.037[b]
Coesite 2	8	24	274.0	2.92	4.17	5.24	4.59	8.19	5.10	676	85	107	167	121	86	794	16/16	1200	0.074	1162	0.037	1117	0.074	1080	0.037[b]
Stishovite 1	2	6	46.5	4.20	5.05	6.16	5.50	11.00	6.16	921	186	227	405	330	233	950	16/16								
Stishovite 2	2	6	46.5	4.20	5.05	6.16	5.50	11.00	6.16	921	186	227	405	330	233	769	16/16	920	0.22						
Rutile 1	2	6	62.4	4.26	4.73	5.73	5.14	9.26	5.72	781	158	191	309	113	80	824	16/16								
Rutile 2	2	6	62.4	4.26	4.73	5.73	5.14	9.26	5.72	781	158	191	309	113	80	500	16/16	610	0.055	824	0.167				
Albite	2	26	332.5	2.62	2.98	3.91	3.33	6.06	3.70	472	57	75	116	82	63	476	23/16	1123	0.154	1010	0.051	750	0.154	625	0.051[b]
Microcline	2	26	360.9	2.56	3.02	3.85	3.34	6.02	3.72	460	56	72	112	74	62	463	39/16	1123	0.154	1010	0.051	750	0.154	625	0.051[b]
Anorthite	2	26	334.5	2.76	3.28	4.30	(3.66)	6.67	4.07	518	62	82	127	100	84	483	40/16	1100	0.154	990	0.051	750	0.154	625	0.051[b]
Clinoenstatite	8	40	417.9	3.21	4.69	4.86	4.76	7.85	5.27	719	83	86	139	190	147	535	24/16	1000	0.100	900	0.100	700	0.067		
Orthoenstatite	16	80	835.0	3.21	4.69	4.86	4.76	7.85	5.27	719	66	68	110	190	147	545	24/16	1000	0.100	900	0.100	700	0.067		
Diopside	2	20	219.5	3.28	4.21	4.58	4.38	7.70	4.87	654	92	101	169	152	129	557	40/16	1000	0.100	900	0.100	650	0.067		
Jadeite	2	20	202.5	3.30	4.57	4.96	4.75	8.19	5.27	724	103	112	185	152	117	615	23/16	1000	0.100	900	0.100	730	0.067		
Tremolite	1	41	453.0	2.98	3.70	3.70	3.70	6.17	4.09	547	64	64	106	150	127	545	40/16	1050	0.089	950	0.089	700	0.081	3677	0.016
Muscovite	2	42	467.0	2.83	3.21	4.02	3.53	5.78	3.90	520	55	69	99	108	91	620	39/16	1000	0.159	800	0.095			3633	0.032
Talc	2	42	452	2.79	3.21	4.02	3.53	5.78	3.90	525	55	69	100	170	132	620	24/16	1000	0.159	800	0.095			3677	0.032
Calcite	2	10	122.6	2.71	2.93	3.70	3.23	6.53	3.62	468	78	99	174	92	71	345	60/40	1460	0.133	1070	0.067	881	0.067	712	0.133
Zircon	2	12	130.5	4.70	3.71	4.33	3.97	8.06	4.46	601	97	113	210	201	142	608	91/90	974	0.055	1000	0.110	885	0.055		
Forsterite	4	28	290.0	3.21	4.90	4.96	4.93	8.56	5.48	747	98	99	171	144	128	620	92/24	930	0.142	837	0.048				
Pyrope	4	80	752.0	3.58	5.05	5.05	5.05	8.96	5.62	794	73	73	130	149	115	630	24/16	975	0.150	875	0.050				
Grossular	4	80	932.0	3.59	5.43	5.43	5.43	9.31	6.02	821	74	74	126	180	152	619	40/16	950	0.150	850	0.050				
Almandine	4	80	765.0	4.32	4.68	4.68	4.68	8.42	5.21	731	68	68	122	117	103	635	56/16	975	0.15	875	0.05				
Spessartine	4	80	790.0	4.19	4.80	4.80	4.80	8.47	5.34	742	69	69	121	113	100	631	55/16	965	0.15	865	0.05				
Andradite	4	80	874.4	3.86	4.96	4.96	4.96	8.47	5.50	738	69	69	117	132	112	589	40/16	925	0.15	825	0.05				
Kyanite	4	32	292	3.67	5.52	6.05	5.76	10.80	6.43	916	110	121	215	237	188	720	27/16	950	0.167						
Andalusite	4	32	342	3.14	4.83	5.29	5.04	9.45	5.63	761	91	100	179	156	124	780	27/16	950	0.167						
Sillimanite	4	32	331	3.25	4.91	5.37	5.20	9.75	5.72	782	94	103	187	115	91	955	27/16	1185	0.041						

For vitreous silica, CRN refers to the continuous random network, and PD to the pentagonal dodecahedral model (see paper 3, p. 50). Where there is no entry in the table, the model did not include the parameter.

[a] The value of $w_l(K = 0)$ for spinel was changed from 225 cm^{-1}, used in paper 3, to 311 cm^{-1}, based on a reevaluation of spinel data, particularly on discussions by *O'Horo et al.* [1973] and *Preudhomme and Tarte* [1971].

[b] The antisymmetric Si-O-Si stretching modes are better defined here than in the model used in paper 3.

The data required by the model are (1) acoustic velocities, which determine the slopes of the acoustic branches, (2) limiting spectral frequencies for the lower and upper ends of the optic continuum, (3) weighting factors and frequencies for any Einstein oscillators used, and (4) densities and volumes of the minerals. Recommended values of these parameters for all minerals considered in this study are given in Table 1. The model is independent of calorimetric data, and the parameters are not obtained by any fitting procedure. All equations for the assumed spectra and the thermodynamic functions are given in paper 3. Corrections to errors in papers 1–3 are given in Appendix C. Discussion of the calculation of acoustic velocities and choice of the limiting spectral frequencies is given in papers 1 and 2. In the following discussions of individual minerals these parameters are discussed in some detail; their choice by careful evaluation of existing literature values determines the accuracy obtained by the model.

3. ORTHOSILICATES AND CALCITE

General Spectral Properties

A study of the lattice vibrational characteristics of the orthosilicates and their influence on the thermodynamic properties provides a key to the understanding of the spectra and thermodynamic behavior of more complex silicates, because spectral characteristics of the orthosilicates are relatively more easily interpreted than those of silicates of intermediate polymerization. From orthosilicate spectra it is possible to estimate the range of frequencies encompassed by Si-O stretching modes and O-Si-O bending modes, to determine the extent to which these vibrational modes are modified by cation-oxygen forces and to judge the extent to which the vibrations of the SiO_4^{-4} tetrahedra can be considered as being distinct from vibrations involving translations of the cation or translations and rotations of the anions [e.g., *Farmer*, 1974*a*, p. 285].

For enumeration of the internal modes of orthosilicates the SiO_4^{-4} tetrahedra can be treated as perturbed anions [*Farmer*, 1974*a*, p. 285]. An isolated tetrahedral SiO_4^{-4} unit would have nine internal degrees of freedom (15 total degrees of freedom, six external modes) but only four distinct modes of vibration because of degeneracy. These vibrations and their frequencies are usually designated as follows: the symmetric stretch ν_1, the doubly degenerate bend ν_2, the triply degenerate stretch ν_3, and the triply degenerate bend ν_4. The form of the vibrational modes is given by *Herzberg* [1945, p. 100].

If the full symmetry of the tetrahedron is preserved, only the ν_3 and ν_4 modes are infrared-active. However, the full symmetry of the isolated tetrahedron is seldom preserved in real minerals, and other modes are frequently infrared-active. Perhaps the best understood and most reliably assigned spectral modes are those of zircon (for which both single-crystal infrared and Raman data are available and in which the perturbing effect of the large and heavy cation is small) and of forsterite. Even for an intensively studied mineral such as forsterite a substantial disagreement in the mode assignments is obtained with the two major methods of analysis: normal-coordinate analysis versus group vibration analysis using the vibrations of the SiO_4^{-4} tetrahedra and metal coordination polyhedra [see *Oehler and Günthard*, 1969; *Iishi*, 1978].

Zircon

The crystallographic unit cell of zircon ($ZrSiO_4$) is tetragonal, *I4/amd*, and contains four $ZrSiO_4$ units. However, the primitive unit cell contains only two formula units and hence 12 atoms and 36 degrees of freedom. The volume of the primitive cell was taken as 130.5×10^{-24} cm^{-3}.

The acoustic velocities used in the model are as follows: $v_{VRH,P} = 8.06$, $v_{VRH,S} = 3.97$, $u_1 = 3.71$, and $u_2 = 4.33$ km s^{-1} [*Simmons and Wang*, 1971, 22252, p. 300; from *Ryzhova et al.*, 1966]. In these papers, $v_{VRH,P}$ and $v_{VRH,S}$ are the Voigt-Reuss-Hill (VRH) longitudinal and shear velocities, respectively (see paper 1 for a discussion of acoustic velocities and their averages); u_1 and u_2 are directionally averaged slow and fast shear velocities, respectively. These averaged shear velocities were obtained by the method described in paper 1 from measured minimum and maximum shear velocities of 2.94 and 4.87 km s^{-1}. The directionally averaged longitudinal velocity u_3 was taken equal to $v_{VRH,P}$. (Two older published shear velocities on zircon are anomalously low in comparison with the Ryzhova values: $v_S = 2.195$ km s^{-1} [*Hearmon*, 1956] and $v_S = 3.200$ km s^{-1} [*Bhimasenachar and Venkataratnam*, 1955]. The Ryzhova value of 3.972 km s^{-1} is more in accord with values expected for v_S of zircon on the basis of velocity-density systematics [*Shankland and Chung*, 1974].) The chosen acoustic velocities give a mean sound speed of 4.46 km s^{-1} and an elastic Debye temperature of 601°K. The acoustic shear branches reach $w_1 = 97$ cm^{-1} and $w_2 = 113$ cm^{-1} at the Brillouin zone boundary, and the longitudinal branch reaches $w_3 = 210$ cm^{-1} (w_1, w_2, and w_3 refer to the cutoff 'frequencies,' specified as wave numbers in cm^{-1}, of the directionally averaged slow and fast shear branches and longitudinal branch, respectively.)

The vibrational spectrum of zircon has been studied in detail by *Dawson et al.* [1971] (see notes for Table 4, paper 2). The eight stretching modes (see Table 6, paper 2) constitute 22% of the total modes. One mode (5.5%) is at 974 cm^{-1}, one mode (5.5%) is at 885 cm^{-1}, and it is assumed that the remaining modes (11.0%) are at 1000 cm^{-1}. These eight modes are represented by Einstein oscillators at these three positions.

The remaining modes are between 608 cm^{-1} (O-Si-O bending vibrations) and 201 cm^{-1} (Zr + SiO_4^{-4} deformations which resemble acoustic modes in that they 'involve shearing displacements of alternating columns or sheets of the structure relative to each other with Zr^{+4} and SiO_4^{-4} moving in the same direction within each column or sheet' [*Farmer*, 1974*a*, p. 287]). The dispersion assumed across the Brillouin zone lowers the frequency of 201 cm^{-1} at the zone center to 185 cm^{-1} at the zone boundary. For the dispersion curve, m_1 was taken as the mass of the SiO_4^{-4} group, and m_2 as the mass of the zirconium because of Farmer's and Dawson et al.'s assignments of low-frequency modes showing the tetrahedra moving as rigid bodies.

The results of the model calculation are given in Figure 2*a*, where C_V values are compared with values derived from data of *Kelley* [1941] below 300°K and *Janaf* [1965*a*, *b*, 1966, 1967] above 300°K. Calorimetric Debye temperatures $\theta_{cal}(T)$ for experimental data and for model values are shown in Figure 2*b*; see paper 1 for an explanation of $\theta_{cal}(T)$. The fit is excellent; for example, at 298°K, C_V*, inferred from measured C_P*, is 3.90 cal mole^{-1} °K^{-1}; the model value is also 3.90 cal mole^{-1} °K^{-1}. At 800°K, C_V* from C_P* data is 5.47 cal mole^{-1} °K^{-1}, whereas the model value is 5.50 cal mole^{-1} °K^{-1}. At values between 298° and 800°K the model slightly underestimates C_V*. (A very large scatter in measured values of thermal expansion [see *Touloukian and Ho*, 1977] makes the C_P-C_V correction difficult to estimate.)

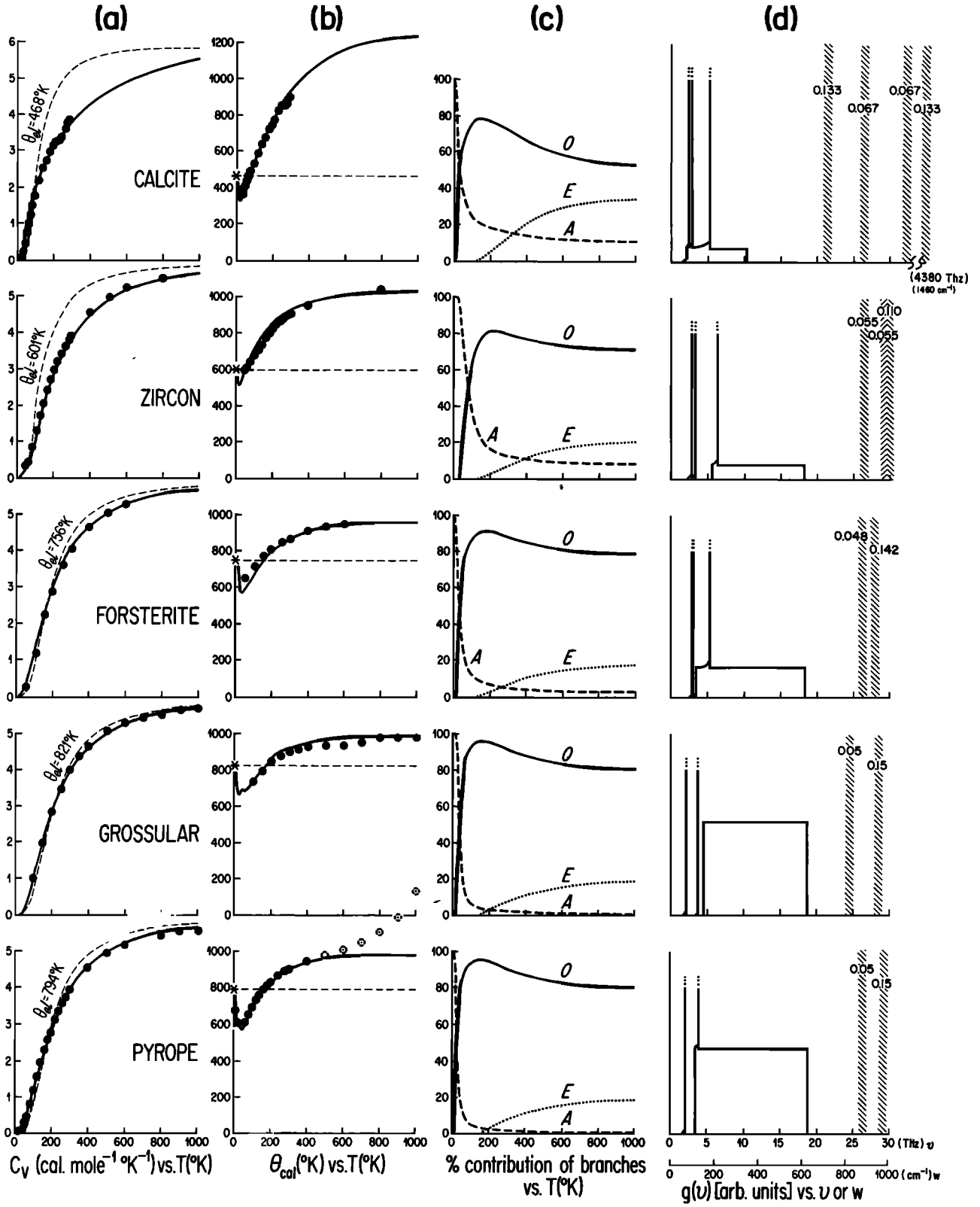

Fig. 2. Data and model values for calcite, zircon, forsterite, grossular, and pyrope. (*a*) Heat capacities as a function of temperature. (*b*) Calorimetric Debye temperatures as a function of temperature. (*c*) Percent contributions to heat capacity of acoustic modes *A*, optic continuum *O*, and Einstein oscillator(s) *E* as a function of temperature. (*d*) Model spectra. The vertical scales shown on the spectra in Figures 2–4 are arbitrary. The singularites in the acoustic branches at ν_1, ν_2, and ν_3 are shown by the three dots on the acoustic branches. Parameters used in the model are given in Table 1. References to heat capacity data are given in Figure 4 of paper 1 as well as in the text. References to spectral data are given in paper 2.

Forsterite

Forsterite is orthorhombic, belonging to space group *Pbnm*. The primitive unit cell contains four formula units, 28 atoms, and hence has 84 degrees of freedom. The volume of the primitive cell is 290.8×10^{-24} cm^3.

Because of the great importance of olivine as a constituent of the earth's mantle the acoustic properties are well known. For the model the acoustic velocities were taken as $v_P = 8.56$ [*Simmons and Wang*, 1971, 32284, p. 305; from *Kumazawa and Anderson*, 1969], $v_S = 4.93$, $u_1 = 4.90$, and $u_2 = 4.96$ km s^{-1} (determined from $v_{min} = 4.42$ and $v_{max} = 5.00$ [*Verma*, 1960] by the method of paper 1). These velocities give acoustic branches which reach 98, 99, and 171 cm^{-1} at the Brillouin zone boundary. The mean sound speed is 5.48 km s^{-1}, and the elastic Debye temperature is 747°K, in good agreement with *Verma*'s [1960] value of 754°K.

The vibrational spectra of olivines of different composition have been studied by *Tarte* [1965] and others, particularly *Paques-Ledent and Tarte* [1973], *Oehler and Günthard* [1969], *White* [1975], and *Iishi* [1978]. Although these authors disagree considerably on detailed mode assignments (see *Oehler and Günthard* [1969] and *Iishi* [1978] for discussion), the spectrum can be broadly characterized as follows: internal SiO_4^{-4} stretching modes from 825 to 995 cm^{-1}, internal bending modes from about 430 to 620 cm^{-1}, complex modes involving both Mg and Si cations from about 350 to 470 cm^{-1}, and translational modes of the magnesium cations or coordination polyhedra below 350 cm^{-1}.

The 16 high-frequency Si-O stretching modes for the unit cell constitute 19% of the total modes (obtained by the method described in paper 2). They were placed at two frequencies representing the high and low portions of the band between 825 and 995 cm^{-1}: 12 of the modes (or 14.2%) at 930 cm^{-1} and four of the modes (4.8%) at 837 cm^{-1}. The optic continuum was taken to extend from 650 cm^{-1} down to 128.2 cm^{-1}. The lower limit of the optic continuum was obtained by taking the lowest-frequency mode at $\mathbf{K} = 0$ as 144 cm^{-1} (see Table 4 of paper 2) and allowing it to be dispersed across the Brillouin zone by the simple scheme described with masses of 92 and 24. This corresponds to the assumption that the lowest-frequency vibrations can be described as Mg versus SiO_4^{-4} tetrahedra rather than Mg versus O, as would be consistent with the assumption generally used for other minerals. This departure seems somewhat justified by the force constant calculations of *Oehler and Günthard* [1969, p. 4726], which give a Mg-O force constant that is about a factor of 16 lower than the Si-O force constant, and by the calculations of *Iishi* [1978, p. 1205].

The results of the model for forsterite are shown in Figure 2. At temperatures above 100°K the agreement with measured data is excellent. For example, at 298°K the C_V* value predicted by the model is 3.98 cal mole^{-1} °K^{-1}, and that obtained from experimental C_P data corrected to C_V* is 4.00 cal mole^{-1} °K^{-1}. This good agreement extends to high temperatures. At low temperatures (<100°K) the heat capacity is slightly overestimated by the model. Because there is little uncertainty in the acoustic velocities and because optic modes make most of the contribution to the heat capacity in the range of the overestimate, it can probably be inferred that the estimated cutoff of the optic continuum at 128 cm^{-1} is too low and that optic modes do not extend this low. This calculation illustrates that the most unknown and most critical parameter in the model is the distribution of modes in the far-infrared spectral region (at $\mathbf{K} = \mathbf{K}_{max}$, not at $\mathbf{K} = \mathbf{0}$).

As a result of the overestimate of the heat capacity at low temperatures, the entropy is somewhat overestimated; the calculated entropy at 298°K is 3.39 mole^{-1} °K^{-1} (this includes 0.04 cal mole^{-1} °K^{-1} estimated anharmonic contribution (Appendix B), whereas the measured entropy is 3% lower: 3.25 cal mole^{-1} °K^{-1}.

Calcite

Calcite ($CaCO_3$) is the molecular solid most studied. The calcite structure is a distorted NaCl structure [*Bragg et al.*, 1965, p. 128] in which calcium ions replace the sodium ions and the oblate carbonate group replaces the chlorine ions. The oblateness of the carbonate group causes the structure to be rhombohedral instead of cubic. The primitive unit cell contains two $CaCO_3$ formula units, 10 atoms, and therefore has 30 degrees of freedom. The volume of the primitive cell is 122.6×10^{-24} cm^3.

Excellent measurements of acoustic velocities of calcite are available [*Peselnick and Robie*, 1963; *Robie and Edwards*, 1966], including a directionally averaged mean velocity, 3.63 km s^{-1}, and a single directionally averaged shear velocity, 3.23 km s^{-1}. In this study the slow and fast directionally averaged shear velocities determined by the method of paper 1 from this averaged value are $u_1 = 2.93$ and $u_2 = 3.70$ km s^{-1}. The longitudinal velocity was taken as 6.53 km s^{-1}. These velocities give the above mean sound speed and an elastic Debye temperature of 468°K, in close agreement with *Robie and Edward*'s [1966] value of 469°K. The acoustic branches calculated from these velocities, with the assumed sine wave dispersion, reach 78, 99, and 174 cm^{-1} at the Brillouin zone boundary, 2.3, 3.0, and 5.2 THz, respectively. The lower two branches imitate the behavior of the single shear branch shown by *Cowley and Pant* [1973], which reaches about 2.8 THz. The longitudinal branch is somewhat higher than the measured branch, which only reaches 4.3 THz at the zone boundary.

Infrared, Raman, and partial inelastic neutron-scattering (INS) data exist (see the summary of infrared and Raman data by *White* [1974, p. 233] and the INS data of *Cowley and Pant* [1973, p. 4796]; see also Table 4, paper 2). The lowest optical mode is one in which the calcium ions are stationary and the carbonate ions execute a rigid-body rotation in the plane of the ion. The frequency of this mode is 92 cm^{-1} at the zone center ($\mathbf{K} = \mathbf{0}$) and, using the mass m_1 of the carbonate complex and mass m_2 of calcium, drops to 71 cm^{-1} at the zone boundary. The measured dispersion curve, however, is nearly flat across the zone. Therefore the model dispersion curve does not duplicate the measured behavior of the lowest branch but introduces no more than about 25% error in the branch position across the zone. (Interestingly, however, the best fitting shell model of Cowley and Pant, with 10 adjustable parameters, shows this mode decreasing by about the same ratio as my simple sine dispersion curve, although the absolute position of their calculated branch is slightly high because it does not match the observed value of 92 cm^{-1} at $\mathbf{K} = \mathbf{0}$. This problem illustrates the difficulty of predicting mode behavior even with quite complex models of atomic force constants.)

The remaining low-frequency modes of calcite are characterized by motions in which the carbonate groups are displaced toward or away from the calcium cations. These mo-

TABLE 2. Summary of $S_{298.15}$ for Garnets

$S_{298.15}$, cal mole^{-1} °K^{-1}	Comments and Reference
	Grossular
Previous theories	
56.7	*Kolesnik et al.* [1977] (modified Debye model)
59.9	*Saxena* [1976] (entropy-volume)
70.3	*Saxena* [1976] (oxide summation)
Experimental	
62.0	*Haselton and Westrum* [1979]
61.6	*Westrum et al.* [1979]
Model	
60.4	
	Pyrope
Previous theories	
47.5	*Saxena* [1976] (entropy-volume)
47.1	*Cantor* [1977] (entropy-mass-volume)
61.1	*Saxena* [1976] (oxide summation)
Experimental	
63.6	*Haselton and Westrum* [1979]
64.0	*Newton et al.* [1977]
66.0	*Kolesnik et al.* [1977]
(61.7)	*Obata* [1976] (inferred by extrapolation from high-temperature)
(58.4 ± 2 or 60.7 ± 2)	*Lane and Ganguly* [1979] (inferred from equilibrium relations)
Model	
65.4	
	Spessartine
Model	
68.2	lattice entropy with (<1%) contribution from anharmonicity added, as described in Appendix B; magnetic spin entropy to be added is 7.21 according to *Ulbrich and Waldbaum* [1976]
	Almandine
Model	
67.0	same as spessartine; magnetic spin entropy to be added is 9.59 according to *Ulbrich and Waldbaum* [1976]
	Andradite
Experimental	
(78.7)	*Kiseleva et al.* [1972]
Model	
70.0	lattice entropy only; magnetic spin entropy to be added is 7.12 according to *Ulbrich and Waldbaum* [1976]

tions produce five infrared-active and two Raman-active lattice modes (shown by *White* [1974, Figure 12.3, p. 231]). Some motions are translational, and others, which correspond to the free rotations of an unbound carbonate molecule, are librational.

The highest-frequency external mode is produced by a stretching motion of the carbonate ion against the calcium ion. The frequencies of the transverse and longitudinal components of this mode are quite different, because the longitudinal frequency is shifted by the long-range polarization field, an effect which is typically large in ionic crystals [*White,* 1974, p. 233]. The wave number of the transverse mode is 303 cm^{-1}, and that of the longitudinal mode is 387 cm^{-1}. A linearly averaged value of 345 cm^{-1} was taken to represent the top of the optic continuum.

In total therefore the external optic modes constitute 15 of the 30 degrees of freedom and are modeled as having frequencies ranging from 72 to 345 cm^{-1}.

The remaining 12 modes are internal vibrations (bending and stretching) of the carbonate ions. The frequencies of these modes depend on interanion coupling but are easily recognized by their similarity to the frequencies of the free carbonate ion. Rather different assignments of the modes can be found in the literature [e.g., *White,* 1974]. I have used here the assignments of *Bottinga* [1968] to facilitate comparison in paper 5 with his results on isotopic fractionation factors. The modes are as follows: 1460 cm^{-1} (four modes), 1070 cm^{-1} (two modes), 881 cm^{-1} (two modes), and 712 cm^{-1} (four modes). Note that both stretching and bending modes of a 'quasi-molecular' unit are isolated from the external modes.

The results of the model are shown in Figure 2, where they are compared with the heat capacity data of *C. T. Anderson* [1934] above 57°K and *Stavely and Linford* [1969] at lower temperatures. The agreement with measured values is excellent. As is shown in Figure 2*c*, at 30°K, acoustic and optic continuum modes contribute equally to C_V; thus the optic continuum modes contribute substantially to the minimum in the $\theta_{cal}(T)$ curve at 25°K. The Einstein oscillator at 712 cm^{-1} begins contributing appreciably to C_V at 200°K and is contributing as much as the acoustic branches by 300°K. At high temperatures the Einstein oscillators account for 40% of the heat capacity.

Garnets

The garnet family is one for which very few heat capacity measurements have been published and for which the few published experimental and theoretical values of heat capacity and entropy disagree so substantially that considerable speculation has arisen regarding the cause of the differences in measured thermodynamic properties from those expected. Five garnets are included in the present study: grossular ($Ca_3Al_2Si_3O_{12}$), pyrope ($Mg_3Al_2Si_3O_{12}$), almandine ($Fe_3Al_2Si_3O_{12}$), spessartine ($Mn_3Al_2Si_3O_{12}$), and andradite ($Ca_3Fe_2Si_3O_{12}$).

The garnet problem specifically concerns pyrope and grossular and can be summarized as follows: The entropy-estimating schemes which exist for minerals give widely disagreeing values for pyrope and grossular (see Table 2). In the case of grossular the oxide summation method overestimates the entropy. For pyrope there is a similar disagreement between the oxide summation scheme and the other schemes. The general conclusion from the estimating schemes is that a lower entropy S would be expected for pyrope (S_{298} = 47 cal mole^{-1} °K^{-1}) than for grossular (S_{298} = 57–60 cal mole^{-1} °K^{-1}). Measured entropies, however, disagree with these theoretical predictions: measured values of S_{298} for grossular are about 62 cal mole^{-1} °K^{-1}, whereas those for pyrope range from 63 to 66 cal mole^{-1} °K^{-1} (Table 1). This lack of agreement between the predicted and the measured values has given rise to the controversy over the 'pyrope excess entropy' [*Newton et al.,* 1977]. A further indication of the complexity of the problem is the fact that the elastic Debye temperature of grossular is higher (821°K) than that of pyrope (794°K), from which a simple Debye model would indicate that pyrope would indeed have the higher entropy at 298°K but should also have a higher heat capacity at any temperature. In fact, even though the entropy of pyrope is greater than that of grossular at 298°K, its heat capacity is less (76–78 cal mole^{-1} °K^{-1} for pyrope compared with 79–82 cal mole^{-1} °K^{-1} for grossular). It will be demonstrated below that these trends are

to be expected from the observed spectroscopic characteristics of the garnets.

The crystallographic unit cell of the garnets is cubic (*Ia3d*), and the primitive unit cell of the garnets therefore contains four formula units and hence 80 atoms and 240 degrees of freedom. The primitive cell volumes used in the model are as follows: grossular, 932×10^{-24} cm^3; andradite, 874.4×10^{-24} cm^3; pyrope, 752×10^{-24} cm^3; spessartine, 790×10^{-24} cm^3; and almandine, 765×10^{-24} cm^3.

Acoustic properties of garnets have been determined by several investigators [*Isaak and Graham,* 1976; *Wang and Simmons,* 1974; *Bonczar et al.,* 1977; *Ryzhova et al.,* 1966; *Babushka et al.,* 1978; *Goto et al.,* 1976]. Garnets are nearly isotropic, and it was therefore assumed in the model that the slow and fast shear velocities are identical (the three acoustic modes account for 3/240 degrees of freedom, so that small uncertainties in the acoustic mode parameters are not important in the calculation of the thermodynamic properties). The velocities used were taken from *Isaak and Graham* [1976] for grossular, pyrope, almandine, and spessartine and from *Babushka et al.* [1978] for andradite. The velocities used are as follows: grossular, $v_S = 5.43$, $v_P = 9.31$ km s^{-1}; andradite, $v_S = 4.96$, $v_P = 8.47$ km s^{-1}; pyrope, $v_S = 5.05$, $v_P = 8.96$ km s^{-1}; spessartine, $v_S = 4.80$, $v_P = 8.47$ km s^{-1}; and almandine, $v_S = 4.68$, $v_P = 8.42$ km s^{-1}. These velocities gave the following mean sound speeds and Debye temperatures: grossular, $v_m = 6.02$ km s^{-1}, $\theta_{el} = 821$°K; andradite, $v_m = 5.50$ km s^{-1}, $\theta_{el} = 738$°K; pyrope, $v_m = 5.62$ km s^{-1}, $\theta_{el} = 794$°K; spessartine, $v_m = 5.34$ km s^{-1}, $\theta_{el} = 742$°K; and almandine, $v_m = 5.21$ km s^{-1}, $\theta_{el} = 731$°K. (Note that from a Debye model based on elastic Debye temperatures the heat capacities, at any temperature, would be expected to increase in the following order: grossular, pyrope, spessartine, andradite, and almandine.) These acoustic velocities and the above cell parameters give acoustic branches truncated at relatively low frequencies at the Brillouin zone boundary (see Figure 1*a*): 74, 74, and 126 cm^{-1} for the two shear branches and one longitudinal branch of grossular; 73, 73, and 130 cm^{-1} for pyrope; 69, 69, and 121 cm^{-1} for spessartine; 68, 68, and 122 cm^{-1} for almandine; and 69, 69, and 117 cm^{-1} for andradite.

Unfortunately, all optical spectra published have been on natural garnets, which have appreciable solid solutions of non-end-member cations. There are therefore some uncertainties in assignment of the optic mode frequencies to given atomic vibrations. Because I wished to compare model C_V values with C_V values obtained from C_P data for pure end-member compositions, it was necessary to attempt to extrapolate the spectra on solid solutions to obtain parameters representative of the pure end-member compositions.

Identifying the Si-O stretching modes of the garnets is relatively easy, because the IR-active modes are isolated from other modes between about 850 and 950 cm^{-1} in a band which has a common shape for all end-member compositions [see *Farmer,* 1974*a*, Figure 13.4, p. 291]. Available Raman spectra show the Raman-active stretching modes from about 700 to 900 cm^{-1} [*Moore et al.,* 1971, p. 65]. *Tarte* [1965], *Moore et al.* [1971], and others have noted a linear relationship between the frequencies of the high-frequency infrared and Raman bands and the lattice parameter. This relationship is apparently due to changes in the Si-O tetrahedral bond lengths for different compositions. In the model, two bands were used to represent the Si-O stretching modes: a high-frequency band containing 15% of the modes and a lower-frequency band containing 5%. The bands are placed at 975 and 875 cm^{-1} for almandine, 975 and 875 cm^{-1} for pyrope, 965 and 865 cm^{-1} for spessartine, 950 and 850 cm^{-1} for grossular, and 925 and 825 cm^{-1} for andradite.

The top of the optic continuum is similarly well defined from infrared spectra [*Moore et al.,* 1971, p. 58; W. B. White, personal communication, 1979; paper 2, Table 4]. It is taken at 619 cm^{-1} for grossular, 630 cm^{-1} for pyrope, 631 cm^{-1} for spessartine, 635 cm^{-1} for almandine, and 589 cm^{-1} for andradite. The position of the bands at the top of the optic continuum does not change significantly for those garnets with aluminum in the octahedral site but is substantially lower for andradite, which has iron in the octahedral site. This suggests that the mode at the top of the optic continuum is an RO_6 octahedral mode, as suggested by *Omori* [1971*a*, p. 843], rather than a ν_2 or ν_4 SiO_4^{-4} mode, as suggested by *Moore et al.* [1971]. The above values were not extrapolated to those appropriate to end-member compositions, as such an extrapolation would lead to a frequency change of only a few wave numbers and would have negligible influence on the thermodynamic properties.

The major problem is selection of the lowest extent of the optic modes, because these modes, although they are largely determined by the eightfold coordinated A cations (where A is Ca, Mg, Fe, and Mn in the end-members and is a mixture of these atoms in the solid solutions observed spectrally), are possibly coupled to the modes of the sixfold coordinated B cations. For the purest grossular samples examined by *Moore et al.* [1971] the lowest mode was at 180 cm^{-1}; these samples had less than 1% almandine. Some grossular samples containing 4–6% almandine (i.e., iron in the A site) showed modes at 140–150 and 117–125 cm^{-1}. These modes are also observed in the purest almandine samples, and I therefore attributed the 117-cm^{-1} mode to the almandine component and used it in the model as the lowest mode frequency for almandine. Spessartine shows a mode at 113 cm^{-1}, close to the almandine value, as would be expected from the similarity of the iron and manganese atoms. The pyrope examined by *Moore et al.* [1971] also had a significant almandine content (16% and 38%) and showed a low-frequency line at 125 cm^{-1}, which I interpret as arising from the impurity Fe vibrations. I have therefore taken the next higher observed line at 149 cm^{-1} as the lowest vibration characteristic of a pure pyrope garnet. The lowest mode of andradite observed in both the *Kieffer* [1979*b*] spectrum and the *Moore et al.* [1971] spectra is at 132 cm^{-1}; a line at 113 cm^{-1} would be expected for Fe in the A site if there were no influence of the B site cation, and, in fact, a weak line at 113 cm^{-1} was observed in one sample by *Moore et al.* [1971]. However, because the line was weak and not reproduced in either Kieffer's or Moore et al.'s work on other andradites, the higher value of 132 cm^{-1} is used in the calculation here.

In summary, then, the zone center value of the lower cutoff of the optic continuum for the garnets was taken as follows: grossular, 180 cm^{-1}; pyrope, 149 cm^{-1}; andradite, 132 cm^{-1}; spessartine, 113 cm^{-1}; and almandine, 117 cm^{-1}. From the dispersion assumed across the Brillouin zone (see paper 3) these modes drop to 152, 115, 112, 99, and 103 cm^{-1}, respectively, at the zone edge by the assumed dispersion. Because the probable coupling between the modes of the eightfold coordinated A cations and the sixfold coordinated B cations would occur through bridging oxygens, in all cases I used the mass of the heavy cation for m_1 in the assumed dispersion relation and the mass of oxygen for m_2.

The heat capacities predicted by the model are shown in

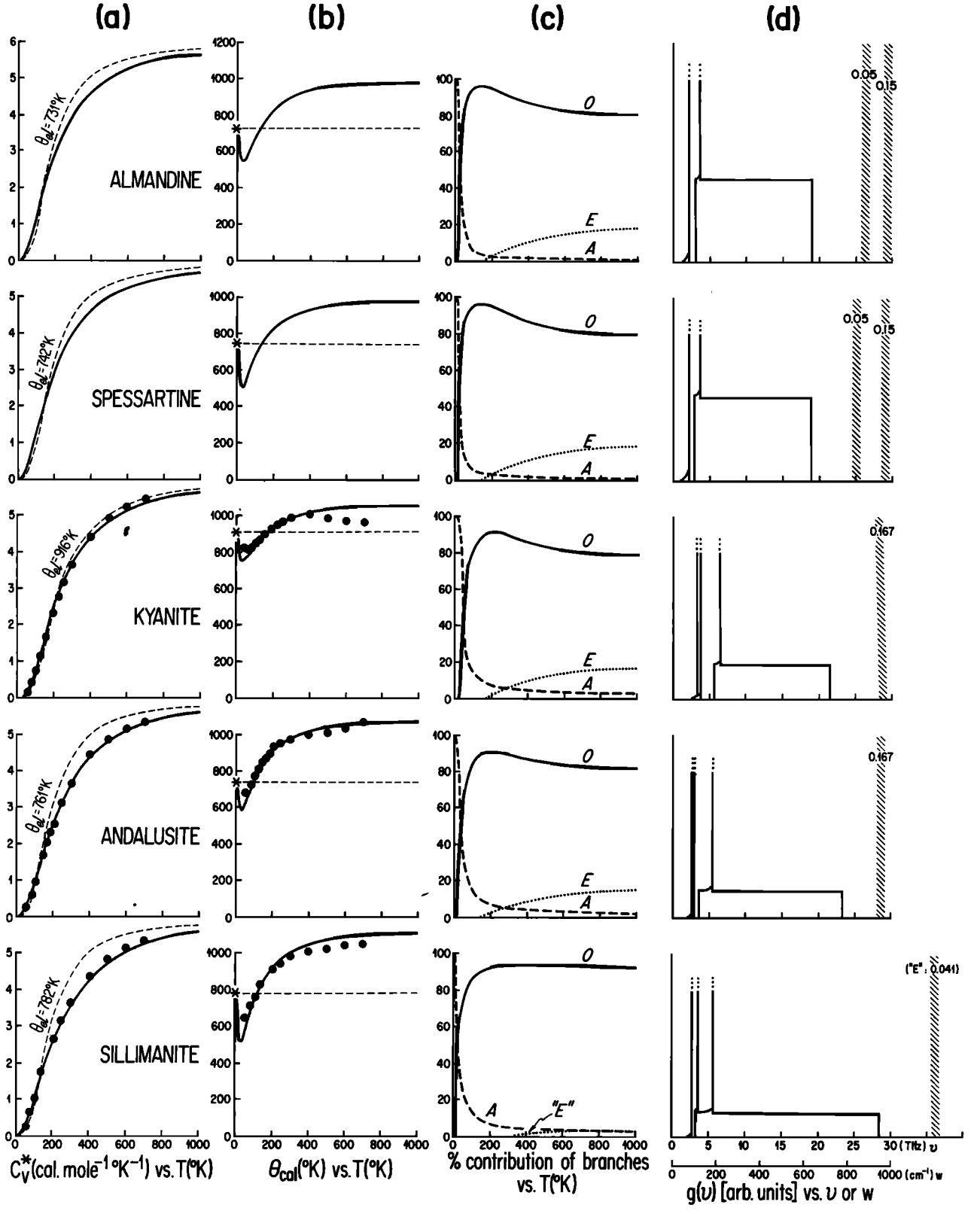

Fig. 3. Data and model values for almandine, spessartine, kyanite, andalusite, and sillimanite. (*a*) Heat capacities as a function of temperature. (*b*) Calorimetric Debye temperatures as a function of temperature. (*c*) Percent contributions to heat capacity of acoustic modes *A*, optic continuum *O*, and Einstein oscillator(s) *E* as a function of temperature. (*d*) Model spectra. The notation is the same as that in Figure 2.

Figure 2 for grossular and pyrope and in Figure 3 for almandine and spessartine. Consider first the model values of the heat capacity C_v^* (normalized to the monatomic equivalent) and calorimetric Debye temperature θ_{cal} (T) of grossular and pyrope and their comparison with experimental values (Figures 2*a* and 2*b*). The experimental values used for pyrope are from *Haselton and Westrum* [1980] (below 350°K) and *Kolesnik et al.* [1977] (above 350°K); the values for grossular from

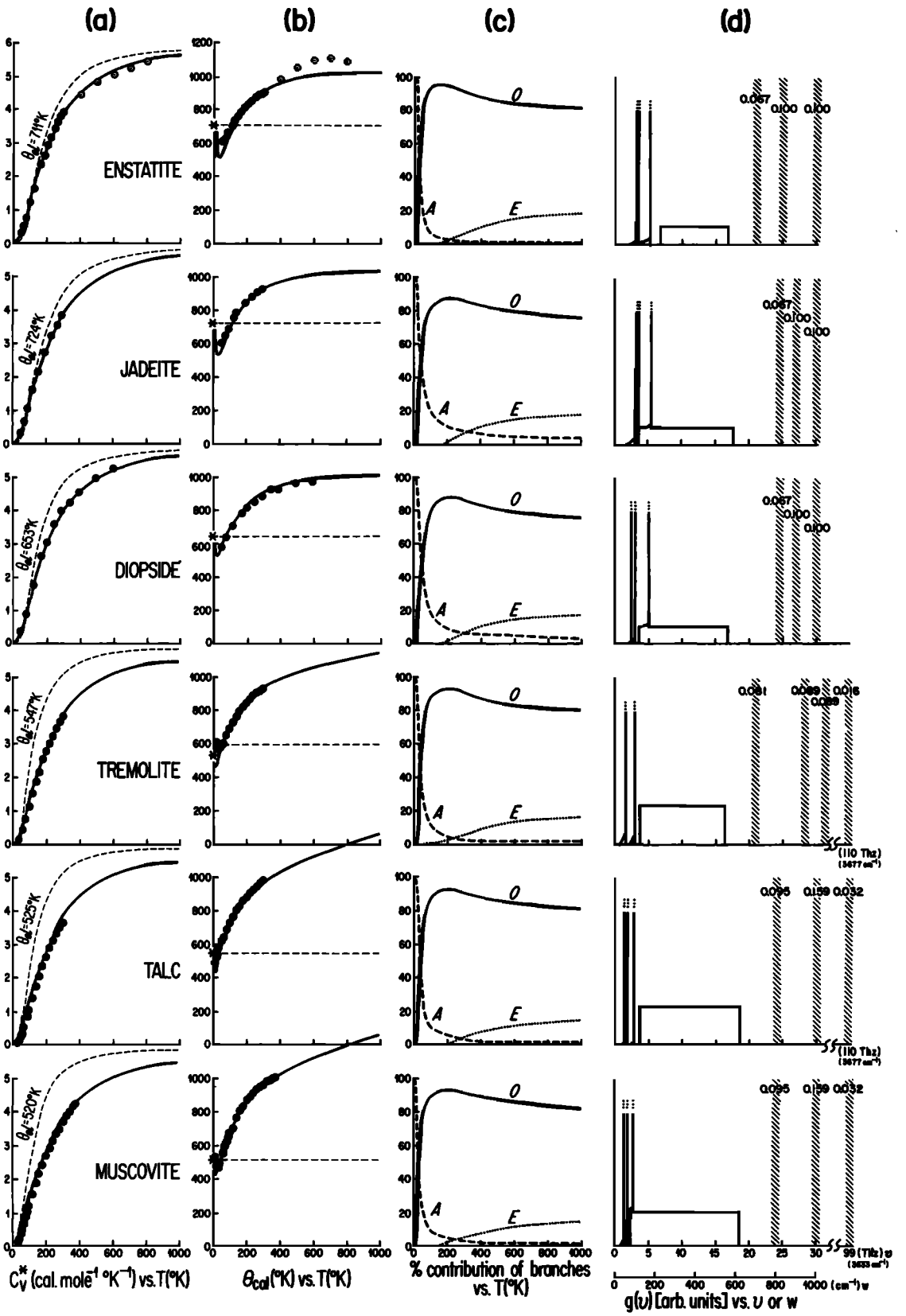

Fig. 4. Data and model values for enstatite, jadeite, diopside, tremolite, talc, and muscovite. (*a*) Heat capacities as a function of temperature. (*b*) Calorimetric Debye temperatures as a function of temperature. (*c*) Percent contributions to heat capacity of acoustic modes *A*, optic continuum *O*, and Einstein oscillator(s) *E* as a function of temperature. (*d*) Model spectra. The notation is the same as that in Figure 2.

300° to 1000°K are from *Krupka et al.* [1979*b*], and the values from 100° to 300°K are from *Westrum et al.* [1979]. *Kolesnik et al.* [1977] also published data below 300°K for pyrope, but the behavior is quite different from the data of Haselton and Westrum and appears anomalous in comparison to the behavior expected from the model and to experimental data on other garnets. Kolesnik's sample was natural pyrope of composition $Py_{71}Al_{18.8}Sp_{0.3}Gr_{8.2}An_{1.9}Uv_{0.2}$, and it is possible that an excess magnetic heat capacity is contributed at low temperatures by iron impurities.

The model predicts a heat capacity C_V^* for grossular of 3.86 cal mole^{-1} °K^{-1}, in fair agreement with measured heat capacities ($C_P^* = 3.94$, $C_V^* = 3.92$ cal mole^{-1} °K^{-1}). The predicted entropy at 298°K, S_{298}^*, is 3.02 (or $S = 60.40$ cal mole^{-1} °K^{-1}), in good agreement with the *Westrum et al.* [1979] value of 61.6 cal mole^{-1} °K^{-1}. For pyrope the model predicts the heat capacity C_V^* at 298°K to be 3.88 cal mole^{-1} °K^{-1}, in good agreement with the measured heat capacity ($C_P^* = 3.89$ or $C_V^* = 3.86$ cal mole^{-1} °K^{-1}), and predicts $S_{298}^* = 3.27$ ($S = 65.40$ cal mole^{-1} °K^{-1}), in good agreement with the measured values, which range from 63.6 to 66.0 cal mole^{-1} °K^{-1}. The model therefore reproduces the observed values of the thermodynamic functions at 298°K within a few percent, and as can be seen in Figure 2, it reproduces measured data well at all temperatures. (The model values of entropy cited above include a correction of ~1% for the anharmonic entropy.)

According to the model spectrum (Figure 2*d*) the pyrope excess entropy (noted on p. 6 of paper 1) is caused by the low-frequency optic modes which extend to 149 cm^{-1} at $\mathbf{K} = \mathbf{0}$ and to 115 cm^{-1} at $\mathbf{K}_{max}$ (the edge of the Brillouin zone), substantially lower than the zone edge value of 152 cm^{-1} for grossular. The lower-frequency modes of pyrope contribute excess heat capacity at low temperatures relative to that for grossular; for example, optic modes contribute 50% of the heat capacity at 30°K for pyrope, whereas for grossular they do not contribute 50% of the heat capacity until nearly 40°K.

A most interesting behavior of the calorimetric Debye temperature curve $\theta_{cal}(T)$ is predicted for grossular at very low temperatures: two minima are predicted, one at 15°K and one at 50°K. If we remember that dips and peaks in the $\theta_{cal}(T)$ curves correspond to peaks and dips, respectively, in the lattice vibrational spectrum, we can see (from Figure 2*d*) that the first minimum is due to the combined *S* and *P* branch singularities and the second minimum is due to the low-frequency modes of the optic continuum. In no other mineral studied have the *S* and *P* acoustic branches been sufficiently separated from the optic continuum to produce this effect, although a similar $\theta_{cal}(T)$ behavior is shown by the experimental data (but not the model) on tremolite (Figure 4). The acoustic modes of grossular are truncated at low frequencies, primarily because the large unit cell gives rise to a small Brillouin zone (see paper 3, equation (16)); the optic modes are at relatively high frequencies, possibly because the large mass difference between the cation (calcium) and anion (oxygen) produces a large stopping band (see paper 1, Figure 8).

The only significant difference between the model vibrational spectra of grossular and pyrope is the much lowered position of the optic modes of pyrope. It is somewhat puzzling that the lowest-frequency mode of pyrope is lower than that of grossular, for these modes are usually associated with cation-oxygen deformations [*Moore et al.*, 1971], and it would be expected that the heavy calcium cations in grossular would have lower vibrational frequencies than the lighter magnesium ions in pyrope. In all garnets the dodecahedrally coordinated cations are surrounded by four 'close' and four 'far' neighbors; for example, in pyrope the magnesium ion has four close neighbors at 2.198 Å and four more distant ones at 2.343 Å [*Gibbs and Smith*, 1965, p. 2033]. However, it has been suggested that the magnesium ion in pyrope lies in a cavity larger than normal for an octahedrally coordinated magnesium ion and that it fills the cavity by a strongly asymmetric vibration [*Gibbs and Smith*, 1965, p. 2033], although the idea of positional disorder has not been substantiated by recent data [*Meagher*, 1975]. Such a strongly asymmetric vibration could give rise to a split-frequency vibrational mode, with the longer bond lengths causing the lowest-frequency mode, which, in turn, causes the excess heat capacity. (A similar asymmetric vibration might account for the low frequency of the Na-O vibration and high low-temperature heat capacity of albite, in which six of the Na-O bonds are between 2.38 and 2.86 Å and two others are at 3.12 and 3.45 Å [*Wyckoff*, 1968; *Winter et al.*, 1977].)

Measured heat capacities and entropies do not exist for almandine, spessartine, and andradite. The predicted values of the harmonic contribution to these functions are given in Table 1 and are shown in Figure 3 for almandine and spessartine. At 298°K the values of C_V^* and S^* (harmonic only) are, respectively, 3.92 and 3.41 cal mole^{-1} °K^{-1} for spessartine, 3.90 and 3.35 cal mole^{-1} °K^{-1} for almandine, and 4.03 and 3.50 cal mole^{-1} °K^{-1} for andradite, with w_i taken as 132 cm^{-1} (reduced to 112 cm^{-1} by the dispersion assumed across the Brillouin zone). If andradite had an Fe vibration at 113 cm^{-1} (reduced to 95.5 cm^{-1} by the assumed dispersion), C_V^* and S^* would be 4.06 and 3.65 cal mole^{-1} °K^{-1}. It can be seen that spectroscopic determination of the far-infrared limits would increase our ability to predict S_{298}^* for andradite; the present uncertainty leads to an uncertainty of about 1.5 cal mole^{-1} °K^{-1} in the estimate of S ($S = S^* \times 20$). Estimated anharmonic contributions are shown in Table 3; in addition, the total entropy must include magnetic and configurational entropy if appropriate. For andradite and spessartine the ideal magnetic spin entropy S_{ms}^* is 0.356 cal mole^{-1} °K^{-1}, and for almandine, S_{ms}^* is 0.480 cal mole^{-1} °K^{-1} [*Ulbrich and Waldbaum*, 1976, p. 4].

Aluminosilicates

The thermodynamic properties of the three aluminosilicate polymorphs kyanite, andalusite, and sillimanite (Al_2SiO_5) are of interest for several reasons: (1) the three phases are common in metamorphic rocks and are therefore used as geothermometers and geobarometers, (2) the position of the triple-point intersection of three univariant equilibrium curves is the subject of considerable controversy and is uncertain because of the very small energy differences amongst the phases [e.g., *Holm and Kleppa*, 1966; *Althaus*, 1967; *Richardson et al.*, 1969; *Holdaway*, 1971; *Zen*, 1972], and (3) in spite of the small thermodynamic differences amongst the phases the optical spectra change considerably from one polymorph to the next. With these polymorphs there is an opportunity to examine the influence of changing coordination of the aluminum cations on spectra and therefore on thermodynamic properties.

All three polymorphs have independent SiO_4^{-4} tetrahedra and are thus generally considered to be orthosilicates. The essential structural difference between the three polymorphic forms is in the coordination of one of the aluminum ions in the Al_2SiO_5 formula unit (see *Bragg et al.* [1965, p. 190] for

TABLE 3. Model Results and Comparison With Experimental Thermodynamic Data

			C_p*		$S_{lattice}$*	
T, °K	C_V*	$TV\epsilon^2B$	Model	Experiment	Model	Experiment
			Halite			
298.15	5.66	0.29[a]	5.95	6.04	8.68	8.62
700	5.90	~0.94	6.86	6.90	14.29	14.09
1000	5.93	~1.58	7.51	7.53	17.04	16.66
			Periclase			
298.15	4.25	0.07	4.32	4.51	3.22	3.22
700	5.57	0.24	5.81	5.82	7.70	7.70
1000	5.76	0.45	6.21	6.12	9.93	9.83
			Brucite			
298.15	3.79	0.01	3.80	3.69	3.45	3.02
400	4.30	0.02	4.32	4.39	4.65	4.21
			Corundum			
298.15	3.78	0.03	3.81	3.77	2.50	2.43
700	5.43	0.15	5.58	5.58	6.67	6.55
1000	5.69	0.31	6.00	5.97	8.82	8.61
			Spinel 1			
298.15	4.00	0.04	4.04	3.96	2.89	2.75
700	5.50	0.12	5.62	5.64	7.14	6.94
1000	5.73	0.21	5.94	6.09	9.23	9.03
			Spinel 2			
298.15	3.89	0.04	3.93	3.96	2.75	2.75
700	5.47	0.12	5.59	5.64	6.94	6.94
1000	5.71	0.21	5.92	6.09	9.03	9.03
			Quartz			
298.15	3.49	0.02	3.51	3.55	3.35	3.30
700	5.16	0.23	5.39	5.50	7.32	7.18
			α-Cristobalite			
298.15	3.47	0.05	3.52	3.52	3.35	3.46
400	4.15	0.05	4.20	4.04	4.47	4.61
			Vitreous Silica (CRN)			
298.15	3.46	0.00	3.46	3.52	3.67	3.82[b]
700	5.16	0.00	5.16	5.18	7.41	7.59
1000	5.53	0.00	5.53	5.60	9.32	9.52
			Vitreous Silica (PD)			
298.15	3.45	0.00	3.45	3.52	3.51	3.82
700	5.15	0.00	5.15	5.18	7.25	7.59
1000	5.53	0.00	5.53	5.60	9.16	9.52
			Coesite 1			
298.15	3.66	0.00	3.66	3.62	3.35	3.22
(700)[c]	5.23	0.02	5.25	5.24	7.23	7.08
(1000)[c]	5.56	0.03	5.59	5.61	9.17	8.96
			Coesite 2			
298.15	3.41	0.00	3.41	3.62	2.99	3.22
(700)[c]	5.15	0.02	5.17	5.24	6.74	7.08
(1000)[c]	5.52	0.03	5.55	5.61	8.65	8.96
			Stishovite 1			
298.15	3.56	0.06[d]	3.62	3.42	2.60	2.21
(700)[c]	5.32	0.18	5.50	5.22	6.62	6.04
(1000)[c]	5.63	0.31	5.94	5.54	8.70	7.96
			Stishovite 2			
298.15	3.48	0.06[d]	3.54	3.42	2.55	2.21
(700)[c]	5.28	0.18	5.46	5.22	6.52	6.04
(1000)[c]	5.60	0.31	5.91	5.54	8.59	7.96

TABLE 3. (continued)

			C_p*		$S_{lattice}$*	
T, °K	C_V*	$TV\epsilon^2B$	Model	Experiment	Model	Experiment
			Rutile 1			
298.15	4.26	0.05	4.31	4.39	4.02	4.01
700	5.54	0.14	5.68	5.48	8.39	8.27
1000	5.75	0.22	5.97	5.83	10.48	10.29
			Rutile 2			
298.15	4.44	0.05	4.49	4.39	4.50	4.01
700	5.57	0.14	5.71	5.48	8.94	8.27
1000	5.76	0.22	5.98	5.83	11.04	10.29
			Albite			
298.15	3.70	0.01	3.71	3.77	3.79	3.81
700	5.25	0.05	5.30	5.34	7.72	7.76
1000	5.58	0.11	5.69	5.74	9.71	9.74
			Microcline			
298.15	3.72	0.00	3.72	3.72	3.86	3.94
700	5.26	0.02	5.28	5.30	7.77	7.84
1000	5.58	0.05	5.63	5.70	9.74	9.81
			Anorthite			
298.15	3.68	0.00	3.68	3.88	3.54	3.66
700	5.26	0.01	5.27	5.45	7.43	7.73
1000	5.59	0.03	5.62	5.87	9.39	9.75
			Clinoenstatite			
298.15	3.92	0.03	3.95	3.92	3.29	3.24
700	5.39	0.09	5.48	5.36	7.41	7.23
(1000)[c]	(5.66)	(0.16)	(5.82)	(5.80)	(9.45)	(9.22)
			Orthoenstatite			
(298.15)[c]	3.88	0.03	3.91	3.92	3.17	3.16
(700)[c]	5.39	0.09	5.48	NA	7.28	NA
1000	5.66	0.16	5.82	NA	9.32	NA
			Diopside			
298.15	3.95	0.03	3.98	3.98	3.49	3.42
700	5.40	0.10	5.50	5.51	7.63	7.56
1000	5.67	0.17	5.84	5.95	9.68	9.60
			Jadeite			
298.15	3.81	0.02	3.83	3.82	3.30	3.19
700	5.36	0.11	5.47	5.40	7.39	7.20
1000	5.65	0.24	5.89	5.83	9.49	9.21
			Tremolite			
298.15	3.87	0.01	3.88	3.82	3.38	3.20
(700)	5.30	0.05	5.35	5.40	7.41	7.23
(1000)	5.58	0.10	5.68	6.07	9.40	9.25
			Muscovite			
298.15	3.68	0.01	3.69	3.71	3.31	3.49
(700)[e]	5.18	0.04	5.22	5.41	7.20	7.44
(1000)[e]	5.49	0.08	5.57	5.83	9.15	9.45
			Talc			
298.15	3.61	0.01	3.62	3.66	2.99	2.97
(700)[e]	5.17	0.04	5.21	5.40	6.85	6.88
			Calcite			
298.15	3.82	0.01	3.83	3.98	4.59	4.38
700	5.16	0.06	5.22	5.46	8.50	8.49
1000	5.51	0.16	5.67	5.95	10.50	10.52
			Zircon			
298.15	3.90	0.01	3.91	3.92	3.44	3.35
700	5.38	0.04	5.42	5.51	7.51	7.45
1000	5.65	0.09	5.74	5.86	9.53	9.49

TABLE 3. (continued)

T, °K	C_V*	$TV\epsilon^2B$	C_p*		$S_{lattice}$*	
			Model	Experiment	Model	Experiment
			Forsterite			
298.15	3.98	0.04	4.02	4.02	3.39	3.25
700	5.43	0.18	5.61	5.55	7.64	7.40
1000	5.69	0.36	6.05	5.99	9.80	9.46
			Pyrope			
298.15	3.88	0.03	9.91	3.89	3.27	3.18[f]
700	5.39	0.10	5.49	5.44	7.38	NA
1000	5.66	0.18	5.84	5.66	9.44	NA
			Grossular			
298.15	3.86	0.02	3.88	3.94	3.02	3.05
700	5.39	0.10	5.49	5.53	7.14	7.20
1000	5.67	0.19	5.86	5.88	9.21	9.24
			Almandine			
298.15	3.90	0.02	3.92	NA	3.35	NA
700	5.39	0.09	5.48	NA	7.48	NA
1000	5.66	0.20	5.86	NA	9.56	NA
			Spessartine			
298.15	3.92	0.02	3.94	NA	3.41	NA
700	5.40	0.12	5.52	NA	7.58	NA
1000	5.67	0.28	5.95	NA	9.68	NA
			Andradite			
298.15	4.03	0.03	4.06	NA	3.50	NA
700	5.45	0.10	5.55	NA	7.70	NA
1000	5.69	0.19	5.88	NA	9.78	NA
			Kyanite			
298.15	3.63	0.02	3.65	3.64	2.60	2.50
700	5.33	0.14	5.47	5.46	6.65	6.50
1000	5.63	0.34	5.97	5.85	8.81	8.52
			Andalusite			
298.15	3.62	0.03	3.65	3.67	2.89	2.79
700	5.32	0.20	5.52	5.43	6.98	6.77
1000	5.63	0.50[d]	6.13	5.80	9.24	8.88
			Sillimanite			
298.15	3.56	0.01	3.57	3.66	2.95	2.87
700	5.28	0.07	5.35	5.33	6.88	6.83
1000	5.60	0.17	5.77	5.78	8.93	8.81

NA means not available. For vitreous silica, CRN refers to the continuous random network, and PD to the pentagonal dodecahedral model (see paper 3, p. 50). All units are cal mole^{-1} °K^{-1}.

[a] The anharmonicity is large; $TV\epsilon^2B$ was calculated from the high-temperature C_p* minus the Dulong-Petit limit for C_V*.

[b] *Janaf* [1965*a*, *b*, 1966, 1967] data were used.

[c] Metastable at these temperatures.

[d] Anharmonic correction very uncertain.

[e] Onset of dehydration may affect C_P* or affect the thermal expansion so strongly that the $TV\epsilon^2B$ term is unknown.

[f] Data below 350°K are from *Haselton and Westrum* [1980].

discussion and illustrations of the structures). In all three polymorphs, one aluminum cation is always in sixfold coordination, and the silicon atom is always in fourfold coordination. In sillimanite the other aluminum is in fourfold coordination; in andalusite, fivefold; and in kyanite, sixfold. The aluminum and oxygen atoms form chains of octahedra of different orientations in the three polymorphs; the variation of the lateral linkages of the chains gives rise to the structural differences.

The polymorphs have identical unit-cell contents but different crystal symmetries. Kyanite is triclinic, $P\bar{1}$, containing four formula units per primitive cell. The unit-cell volume was taken as 292 × 10^{-24} cm^3. Andalusite is orthorhombic, *Pnnm*, containing four formula units per primitive cell. The unit-cell volume was taken as 342 × 10^{-24} cm^3. Sillimanite is also orthorhombic, *Pbnm*, containing four formula units per primitive cell. The cell volume was taken as 331 × 10^{-24} cm^3. The unit cells of all three polymorphs contain 32 atoms and hence have 96 degrees of freedom.

Acoustic velocities have been measured only on sillimanite [*Simmons*, 1964*a*, *b*]. From these data I estimated the slow and fast directionally averaged shear velocities to be u_1 = 4.91 and u_2 = 5.37 km s^{-1} and the directionally averaged longitudinal velocity to be 9.75 km s^{-1}, giving a mean sound speed of 5.72 km s^{-1} and an elastic Debye temperature θ of 782°K. I then used the relations v_P/ρ = const = 3.0 and v_S/ρ = const = 1.58

to estimate the shear and longitudinal velocities for andalusite and kyanite. This scheme [*O. L. Anderson,* 1965] gave v_S = 5.04 and v_P = 9.45 km s^{-1} for andalusite; I assumed that the degree of anisotropy was the same for all polymorphs, that is, that u_1/v_S = const and u_2/v_S = const. This gave u_1 = 4.83 and u_2 = 5.29 km s^{-1} for andalusite, v_m = 5.63 km s^{-1}, and θ_{el} = 761°K. For kyanite the same assumptions give v_P = 10.80, v_S = 5.76, u_1 = 5.52, u_2 = 6.05, v_m = 6.43 km s^{-1}, and θ_{el} = 916°K. These estimates of v_m, and therefore θ_{el}, are very close to values obtained by other estimating schemes, such as the equation $\theta_{el} = 164^{4/3}$ [*O. L. Anderson,* 1965], or from the relationship of sound speed to the index of refraction [*O. L. Anderson and R. C. Liebermann,* 1966] and to the new data of *Vaughn and Weidner* [1978]. With these sound speeds and lattice parameters the following acoustic branch cutoff frequencies were obtained: w_1 = 110, w_2 = 121, and w_3 = 215 cm^{-1} for kyanite; w_1 = 91, w_2 = 100, and w_3 = 179 cm^{-1} for andalusite; and w_1 = 94, w_2 = 103, and w_3 = 187 cm^{-1} for sillimanite.

The spectra of these three minerals show marked changes as the coordination number of the aluminum changes. Consider first the spectral characteristics of kyanite and andalusite (discussed in paper 2 and, for andalusite, in a recent paper by *Iishi et al.* [1979]). The Si-O stretching frequencies are quite typical of the orthosilicates, extending from 880 to 1030 cm^{-1} in the infrared spectra. These were modeled as a single Einstein oscillator at 950 cm^{-1}, containing 16.7% of the total modes (see paper 2, Table 6). The SiO_4^{-4} bending modes and the Al-O stretching and bending modes, which normally lie below 650 cm^{-1} in orthosilicates, extend to 720 cm^{-1} in kyanite and to 780 cm^{-1} in andalusite. *Farmer* [1974*a*, p. 293] and *Lazarev* [1972] discuss possible causes of these increased frequencies. The lowest observed optical mode in kyanite is at 237 cm^{-1} (lowered to 188 cm^{-1} by the dispersion assumed across the Brillouin zone) and in andalusite is at 156 cm^{-1} (lowered to 124 cm^{-1} by dispersion across the Brillouin zone).

The spectrum of sillimanite is much more complex than the spectra of kyanite or andalusite. The Si-O stretching vibrations are greatly perturbed by the presence of fourfold coordinated aluminum atoms, which enter into alternating sites in ribbons of tetrahedra which run through the structure parallel to the *c* axis. The Si-O-Al vibrations extend from 650-700 to nearly 1200 cm^{-1}, the latter being possibly the highest frequency observed for Si-O stretching in any mineral. Because of this large range of frequencies covered by the stretching modes it is not possible to isolate the Si-O-Al stretching modes, which, according to paper 2, should constitute 5/24, or 20.8%, of the total degrees of freedom. Four modes (two per sillimanite 'ribbon,' of which there are two per unit cell [*Lazarev,* 1972]) are quite isolated at 1175 and 1195 cm^{-1} (see *Lazarev* [1972, p. 172] for a detailed discussion of the frequencies of the stretching modes of the sillimanite ribbon). These were accordingly modeled as an Einstein oscillator at 1185 cm^{-1} containing 4.2% of the total modes. The remaining optic modes were placed in the optic continuum stretching from 955 down to 91 cm^{-1} (the latter being the 115-cm^{-1} mode observed at **K** = **0** with dispersion asumed across the Brillouin zone).

The general differences in the aluminosilicate spectra caused by the change of coordination are illustrated in the model spectra shown in Figure 3*d*; however, the model spectra are not nearly as detailed or as well based as those of zircon, forsterite, and the garnets discussed earlier. As the coordination of aluminum changes from six to five to four through the sequence kyanite, andalusite, and sillimanite, the optic continuum stretches toward both higher and lower frequencies, ultimately, in sillimanite, encompassing two of the three acoustic branches and most of the Si-O stretching modes.

The heat capacities calculated from the model vibrational spectra are shown in Figure 3. The agreement with the experimental data of *Simon and Zeidler* [1926] is quite good except at low temperatures, where the model overestimates C_V* for all three polymorphs. At 298°K the agreement with measured values is excellent: C_V* (in cal mole^{-1} °K^{-1}) for kyanite is 3.63 (model), 3.63 (experimental); for andalusite is 3.62 (model), 3.65 (experimental); and for sillimanite is 3.56 (model), 3.66 (experimental). The entropies obtained at 298°K, S_{298}* (in cal mole^{-1} °K^{-1}) are as follows: kyanite, 2.60; andalusite, 2.89; and sillimanite, 2.95. The entropies are systematically high (2.7–3.6%) in comparison with experimental values, because the low-temperature heat capacities are overestimated by the model, but the entropy differences between the phases are very close to the measured differences. In terms of entropy per formula unit (as contrasted to the monatomic equivalent given above) the entropy differences are as follows: kyanite − andalusite = −2.32, andalusite − sillimanite = −0.48, and kyanite − sillimanite = −2.80 cal mole^{-1} °K^{-1}.

4. CHAIN AND SHEET SILICATES

General Spectral Properties and Enumeration of (Si, Al)-O Stretching Modes

Several problems are encountered in the attempt to formulate model vibrational spectra for the chain and sheet silicates: (1) spectral data and mode assignments are both relatively sparse, (2) the silicon-oxygen stretching modes are complex, consisting of both Si-O-Si bridging modes and Si-O nonbridging modes, and (3) the minerals studied may have a wide range of compositions and impurities, so that interpretation and comparison of data are complicated. Problem 3 makes it difficult to compare the model values, based on spectra of minerals of perhaps one composition, structure, and degree of purity, with calorimetric data, obtained on minerals of possibly different characteristics.

Enumeration of the silicon-oxygen stretching modes was relatively simple for both the framework silicates and the orthosilicates, because in those cases the stretching modes were of a single kind: Si-O-Si or (Si, Al)-O-(Si, Al) bridging modes in the framework silicates and Si-O modes in the orthosilicates. In single-chain, double-chain, and layer silicates these different kinds of modes must be separated and enumerated. Even when the enumeration is accomplished (see discussion below), a problem remains in identifying the frequency ranges of the modes (the different stretching modes lie at different frequencies), because they may overlap Si-O bending modes, cation deformation modes, or, particularly, hydroxyl modes.

The Si-O-Si stretching modes may be characterized as symmetric and antisymmetric modes (see, for example, *Lazarev* [1972] and further discussion below). These two types of modes are found in quite different frequency ranges: the antisymmetric modes typically between 900 and 1100 cm^{-1} and the symmetric modes between 500 and 800 cm^{-1}, depending on the degree of polymerization and aluminum-for-silicon substitution in the tetrahedra. The Si-O stretching modes usually occur at the high frequencies, intermixed with the antisymmetric Si-O-Si modes.

To illustrate problems 1 and 2 listed above, consider muscovite ($KAl_2(AlSi_3O_{10})(OH_2)$), a relatively well studied mineral, and the assignments of the high-frequency bands given by *Velde* [1978], *Farmer* [1974*b*], and *Lazarev* [1972]. The antisymmetric Si-O-Si stretching bands are easily recognized at 1000–1100 cm^{-1}. *Lazarev* [1972, p. 124] assigns the symmetric Si-O-Si vibrations to weak bands at 700–750 cm^{-1}; *Vedder* [1964] places these modes much lower, at 520 cm^{-1}. *Lazarev* [1972] places the Si-O mode in the same range as the antisymmetric Si-O-Si bands. However, other bands are mixed in with these silicon-oxygen stretching modes. A weak band at about 900–950 cm^{-1} (band 5 of *Velde* [1978]) may be an Al-OH^- librational mode, but its existence and interpretation are both subject to controversy [*Velde,* 1978, p. 345]. However, OH^- librational modes between 800 and 950 cm^{-1} appear common to most dioctahedral minerals. In muscovite solid solutions with celadonite ($K(AB)Si_4O_{10}(OH)_2$, where A is Mg and B is Fe [*Farmer,* 1974*b*, p. 351]), but not in pure muscovite, a band at 833 cm^{-1} is attributed to $MgAlOH^-$; in pure muscovite it is replaced at 825 cm^{-1} by the Al-O apical (out of plane) vibration. A band at 805 cm^{-1} is attributed to tetrahedral Al-O-Al vibration, and one at 751 cm^{-1} to Al-O-Si in-plane vibrations. Bands below 697 cm^{-1} are generally not assigned to specific deformations. This extension of the (Si, Al)-O stretching modes to relatively low frequencies (<750 cm^{-1}) and the possibility of their overlap with other modes, in this case the $AlOH^-$ librational modes (at 900–950 cm^{-1}), make difficult the assignment of bands in the region of critical interest for specifying cutoffs for the model. Although the librational modes do not constitute a sufficiently large fraction of the total modes to warrant special treatment in the heat capacity model, for example, by a separate Einstein oscillator, they can cause errors in the calculations if they are mistakenly taken as Si-O stretching modes.

In this paper, enumeration of the silicon-oxygen stretching modes in these minerals is accomplished by using principles formulated by *Lazarev* [1972]. In Lazarev's discussion of the vibrations of groups of coupled silicon-oxygen tetrahedra he states (p. 61) that 'it is appropriate to classify these, not by reference to the "genetical" link with the vibrations of the isolated tetrahedron (as many authors do), but by reference to their preferential association with the vibrations of the Si-O-Si bridges and the terminal Si-O^- and Si-O-Si bonds.' The reader is referred to Lazarev's book for extensive discussion of the principles implied in this short quotation and for applications to specific minerals.

Framework silicates represent the one end-member of this genetical series in which all or nearly all vibrations are of the type Si-O-Si; orthosilicates represent the other end-member, in which all or nearly all vibrations are of the type Si-O^-. For the framework silicates considered in paper 3 it was assumed that all vibrations are of the type (Si, Al)-O-(Si, Al), that there are as many Si-O-Si bonds per unit cell as there are oxygens per unit cell, and that for each Si-O-Si bond there is one symmetric stretch and one antisymmetric stretch. It was assumed that the antisymmetric stretch modes were at much higher frequencies than the symmetric modes (i.e., the antisymmetric modes were the isolated modes represented by the Einstein oscillator(s)), and these were enumerated according to the scheme given in paper 2. In that paper the symmetric modes were included as part of the optic continuum; in the tables at the end of this paper and in the discussion of oxygen isotope fractionation in paper 5 the symmetric Si-O-Si modes are also considered as separately enumerable modes in order to increase the accuracy of the model. For the orthosilicates considered in the previous section it was assumed that all vibrations of the isolated tetrahedra were Si-O modes and that there were four of these modes per tetrahedron in the unit cell.

The Si-O stretching modes of silicates of intermediate polymerization are enumerated as follows.

Layer silicates. For each Si_2O_5 unit in the primitive cell, there are two bonds of the Si-O^- type and three bonds of the Si-O-Si type. These latter bonds give rise to three symmetric and three antisymmetric stretching modes, whereas the former give two stretching modes. Note that the number of 'bonds' defined equals the number of oxygens in the vibrational unit (the Si_2O_5 complex). For this unit there are therefore eight stretching modes. Data presented by *Lazarev* [1972, pp. 117–125] suggest that the Si-O^- and the asymmetric Si-O-Si modes are grouped together in frequency and are at higher frequency than the symmetric stretching modes. Therefore, per Si_2O_5 complex, five modes are assigned to the high-frequency band, and three to the lower-frequency band.

Amphiboles. For each Si_4O_{11} unit in the double chains of the amphiboles, there are four tetrahedra which have five Si-O-Si bonds, two O^--Si-O^- groups, and two Si-O^- groups. The five Si-O-Si bonds give rise to five symmetric and five antisymmetric modes, the two O^--Si-O^- groups give rise to two symmetric and two antisymmetric modes, and the two Si-O^- bonds give rise to two vibrations. Therefore for the Si_4O_{11} complex there are 16 modes. It is reasonable to assume from Lazarev's data and discussion of the 11 modes associated with the antisymmetric Si-O-Si vibrations that the Si-O^- vibrations and both the symmetric and the antisymmetric O^--Si-O^- vibrations lie at much higher frequencies than the five modes of symmetric Si-O-Si vibrations.

Pyroxenes. For each Si_2O_6 unit in the single chains there are two Si-O-Si bonds and four Si-O^- bonds. The Si-O-Si bonds give rise to two symmetric and two antisymmetric vibrations, and the four Si-O^- bonds give rise to four vibrations, a total of eight vibrations per Si_2O_6 unit. It is reasonable to assume that the two antisymmetric Si-O-Si vibrations and the four Si-O^- vibrations are at higher frequencies than the two symmetric Si-O-Si vibrations.

With this scheme for enumerating the stretching vibrations the fraction of the total modes per unit cell associated with the various Si-O modes can be specified. The assignment of frequency ranges to the modes is considered below for the individual minerals.

Pyroxenes and Amphiboles

Study of the pyroxenes and amphiboles clinoenstatite, orthoenstatite, diopside, jadeite, and tremolite allows several correlations and comparisons of the effect of structure and composition on thermodynamic properties: (1) a comparison of the single-chain silicate jadeite ($NaAlSi_2O_6$) with its isochemical equivalent framework mineral, albite ($NaAlSi_3O_8$), shows the effect of structural changes; (2) a comparison of jadeite with diopside ($CaMgSi_2O_6$) shows the effect of ionic substitution in isostructural minerals; (3) a comparison of the properties of orthoenstatite and clinoenstatite ($MgSiO_3$) with each other and with the properties of diopside shows the effect of a doubled unit cell size (although the comparison is complicated by the substitution of a calcium ion in diopside); and (4) a comparison of diopside with tremolite ($Ca_2Mg_5Si_8O_{22}(OH)_2$) shows the effect of single-chain struc-

ture versus double-chain structure and the effect of the addition of a small amount of $(OH)^-$.

Solid-state substitution of cations into the pyroxene lattice and a lack of both far-infrared and Raman spectroscopy on many of the end-member compositions give rise to problems in interpretation of the far-infrared data similar to the problems discussed in section 3 for interpretation of the garnet spectra. Numerous weak lines can be found in reported spectra. If the lowest lines found in published data were to be used, the lowest optic modes for the minerals would be as follows (see paper 2, Table 3): jadeite, 138 cm^{-1}; diopside, 75 cm^{-1}; and orthoenstatite, 140 cm^{-1} (listed erroneously as ~110 cm^{-1} in Table 3 of paper 2). In high-resolution spectra of jadeite and diopside obtained by the author (paper 2, Figure 1) these lowest-frequency bands were not observed, and it seems probable that they are weak impurity lines. Both jadeite and diopside show a strong line at 152 cm^{-1}. *Kovach et al.* [1975] attribute this line, in diopside, to chain deformations. This line is taken as the lowest-frequency optic mode for both substances.

The interpretation of the spectra of orthoenstatite and clinoenstatite is much more difficult. The published infrared spectrum [*Kovach et al.*, 1975, p. 246] and Raman spectrum [*White*, 1975, p. 341] of orthoenstatite show a strong line at 234 cm^{-1}, a weak line on the shoulder of this strong line at 190 cm^{-1}, and a moderate strength line at 140 cm^{-1} (listed erroneously in paper 2, Table 3 as 110 cm^{-1}). There are no low-frequency spectra of clinoenstatite. The Raman spectra of orthoenstatite and pure clinoenstatite are very similar [*White*, 1975, p. 341] from 1000 down to 200 cm^{-1} in spite of some expected differences due to the structural differences of the two polymorphs (see *Lazarev* [1972, p. 102] for a discussion). Therefore one possible assumption would be that the distribution of optic modes is similar in the two substances and that the same lower cutoff should be used for each. However, examination of available spectra [*Kovach et al.*, 1975, pp. 243, 245] on pigeonites, which are structurally similar to clinoenstatite, suggests a different possibility. In pigeonites the lowest-frequency infrared mode in the Mg-Fe rich members is at approximately 200 cm^{-1}. The frequency depends on the Mg/Fe ratio and extrapolates to 235 cm^{-1} for pure clinoenstatite, which is approximately the same frequency as a weak band in the Raman spectrum. The spectrum of a calcium rich pigeonite shown by *Kovach* [1975, p. 243] shows a slight inflection at about 150 cm^{-1}, the position of the strong line in the diopside hedenbergite series associated with chain deformations. Several possible interpretations are raised: that the 235-cm^{-1} line observed in Mg rich pigeonites is the lowest mode in the clinoenstatites, that the 140- to 150-cm^{-1} band (presumably due to chain deformations) is the lowest mode in both enstatites, or that the weak 190-cm^{-1} line is the lowest mode in both enstatites. Available data do not allow a choice between these alternatives, and all three were examined in the models below for the enstatites. Only the model with $w = 190$ cm^{-1} gave results consistent with experimental data, and this value was therefore used. A problem clearly remains, however, in interpreting and reconciling spectroscopic data with calorimetric data.

Orthoenstatite and clinoenstatite. According to *Janaf* [1965*a*, *b*, 1966, 1967] the stable phase of enstatite below 903°K is clinoenstatite, which inverts to orthoenstatite at 903°K and to protoenstatite above 1258°K. *Kelley* [1943] published calorimetric data on clinoenstatite; *Krupka et al.* [1979*a*] have recently published heat capacities and a 298°K entropy for orthoenstatite. The entropy at 298°K of orthoenstatite is 15.77 cal $mole^{-1}$ $°K^{-1}$, lower than that of clinoenstatite at 298°K, 16.21 cal $mole^{-1}$ $°K^{-1}$ [*Krupka et al.*, 1979*a*]. Even given the uncertainties of spectral data discussed above, it is of interest to see if this difference can be understood in terms of the elastic and spectral characteristics of the two polymorphs.

The primitive unit cell of clinoenstatite ($P2_1/c$) contains 40 atoms in a volume of 417.9×10^{-24} cm^3. The primitive unit cell of orthoenstatite (*Pcab*) is twice as large, 834×10^{-24} cm^3, and contains 80 atoms. The acoustic velocities (obtained on orthoenstatite but assumed to be representative of both polymorphs because of their nearly identical densities) are relatively low ($u_1 = 4.69$, $u_2 = 4.86$, and $u_3 = 7.85$ km s^{-1}), giving a mean sound speed of 5.27 km s^{-1} and a Debye temperature of 719°K for both polymorphs. The slow and fast shear and longitudinal acoustic branches reach 83, 86, and 139 cm^{-1}, respectively, at the Brillouin zone boundary of clinoenstatite and 66, 68, and 110 cm^{-1} in orthoenstatite. The higher values for clinoenstatite are obtained because the Brillouin zone is larger than that of orthoenstatite.

At high frequencies the dominant features of the spectra of all pyroxenes are the intense antisymmetric Si-O-Si bands between 800 and 1100 cm^{-1} and the intense bands in the range 650–700 cm^{-1}, characteristic of the symmetric Si-O-Si vibrations. In the model, 10% of the modes (the antisymmetric Si-O-Si modes) were placed at 1000 cm^{-1}, and 10% at 900 cm^{-1}. The symmetric Si-O-Si modes constitute 6.7% of the total modes and were placed at 700 cm^{-1}. The top of the optic continuum was taken as the intense Raman band at 535 cm^{-1} for clinoenstatite and 545 cm^{-1} for orthoenstatite [see *White*, 1975, p. 341], and the bottom of the optic continuum was taken at 190 cm^{-1} for both polymorphs, as discussed above.

Calculations for clinoenstatite are shown in Figure 4, where they are compared with measured data. Data below 300°K are from *Kelley* [1943], and those above 300°K are from *Janaf* [1965*a*, *b*, 1966, 1967]. The model agrees well with measured data at temperatures below 400°K and overestimates the heat capacity by a few percent at higher temperatures. The peculiar behavior of the calorimetric data above 600°K may be due to (1) improper correction of C_P to C_V due to the use of a poor approximation to the thermal expansion (see paper 3), (2) anharmonicity, or (3) the onset of the clino-ortho change at 903°K.

For orthoenstatite the only differences from clinoenstatite were assumed to be (1) the size of the doubled unit cell, the number of atoms in it, and therefore the number of degrees of freedom associated with the unit cell and (2) a slight difference in the frequency of the top of the optic continuum. Acoustic modes constitute only three of the degrees of freedom, and the relative fraction changes from 3/120 for clinoenstatite to 3/240 for orthoenstatite. Because of the reduced Brillouin zone these modes are also reduced to lower frequencies. The net result of these two small changes is a lower heat capacity and 298°K entropy for orthoenstatite: $C_V^* = 3.88$ cal $mole^{-1}$ $°K^{-1}$, and $S^* = 3.17$ cal $mole^{-1}$ $°K^{-1}$. The calculated entropy difference between clinoenstatite and orthoenstatite at 298.15°K is $S^* = 0.12$ cal $mole^{-1}$ $°K^{-1}$, or $S = 0.60$ cal $mole^{-1}$ $°K^{-1}$, slightly higher than the 0.44 cal $mole^{-1}$ $°K^{-1}$ inferred from calorimetry. However, the near agreement of the values based on these considerations suggests that small changes in vibrational mode frequencies due to the poly-

morphic structural differences can account for the entropy differences observed.

Diopside. Diopside ($CaMgSi_2O_6$) is monoclinic (*C2/c*). Therefore the volume of the primitive unit cell is half the volume of the crystallographic cell: $V_L = 219.5 \times 10^{-24}$ cm^3. The primitive cell contains two formula units, 20 atoms, and therefore has 60 degrees of freedom. The acoustic velocities used are $u_1 = 4.21$, $u_2 = 4.58$, and $u_3 = 7.70$ km s^{-1}, giving a mean sound speed of 4.87 km s^{-1} and an elastic Debye temperature of 654°K, substantially lower than the elastic Debye temperature of 719°K for enstatite. The three acoustic branches reach 92, 101, and 169 cm^{-1} at the Brillouin zone boundary.

From the infrared and Raman data available for diopside (summarized in paper 2, Table 3) the antisymmetric Si-O-Si stretching modes were represented in the model by one Einstein oscillator containing 10% of the modes at 900 cm^{-1} and one containing 10% of the modes at 1000 cm^{-1}. An additional Einstein oscillator containing 6.7% of the modes was placed at 650 cm^{-1} to represent the symmetric Si-O-Si modes; the mode appears to be at a lower frequency in diopside than in clinoenstatite. The frequency of the lowest well-documented optical mode for diopside is 150 cm^{-1}. The assumed dispersion drops the frequency of the mode to 127 cm^{-1} at the Brillouin zone center. (Two low-frequency modes reported by *Omori* [1971*b*] at 75 and 140 cm^{-1} were not reproduced in spectra obtained by *Kieffer* [1979*b*]. The 75-cm^{-1} mode may have been a water vapor mode. The mode at 140 cm^{-1} was very weak [*Omori*, 1971*b*, p. 1608]; use of this value (reduced to 118 cm^{-1} by dispersion) in the model changes the heat capacity near 100°K by a few percent but has less than a 1% effect on the value of C_V* at 298°K.)

The model heat capacities are shown in Figure 4, where they are compared with the data of *King* [1957]. At all temperatures the model values match experimental values reasonably well; for example, at 298°K the model value of C_V* is 3.95 cal mole^{-1} °K^{-1}; the value from calorimetric data is 3.95 cal mole^{-1} °K^{-1}. The model S_{298}* is 3.49 cal mole^{-1} °K^{-1} (including a 1% anharmonic term); the experimental value is 3.42 cal mole^{-1} °K^{-1} (based on data above 50°K). The heat capacity is dominated by acoustic branches below 45°K and by optic branches above that temperature. The Si-O stretching modes make a significant contribution to C_V* only above 298°K.

Jadeite. The study of jadeite ($NaAlSi_2O_6$) is of interest for comparison with albite as an isochemical but structurally different material and with diopside as a structurally similar but chemically different substance. For comparison, measured C_P* values at 298.15°K are as follows: jadeite, 3.83; albite, 3.76; and diopside, 3.98 cal mole^{-1} °K^{-1}.

There are 20 atoms in the primitive unit cell (*C2/c*) of volume 202.5×10^{-24} cm^3 and thus 60 degrees of freedom. Three of these are acoustic modes. Acoustic velocities taken from $v_{VRH,P} = 8.19$, $v_{VRH,S} = 4.75$ km s^{-1} [*Horai and Simmons*, 1970] and the assumption that $u_2/v_{VRH,S} = 1.05$ (as for diopside) are $u_1 = 4.57$ and $u_2 = 4.96$ km s^{-1}. These give a mean sound speed of 5.26 km s^{-1} and an elastic Debye temperature of 724°K (compared with $\theta_{el} = 472$°K for albite and 654°K for diopside). Note that the heat capacity relationships given above cannot be explained by the relative Debye temperatures. The three acoustic branches terminate at 103, 112, and 185 cm^{-1} at the Brillouin zone boundary.

Infrared spectral data, but not Raman data, are available for jadeite. The bottom of the optical continuum was taken as 152 cm^{-1} (nearly the same frequency as the lowest observed value for diopside and much higher than the lowest observed mode for albite (83 cm^{-1})). A weak mode at 138 cm^{-1} (paper 2, Figure 1*d*) was ignored as a probable impurity mode. The mode at 152 cm^{-1} is reduced by dispersion (with $m_1 = 23$ and $m_2 = 16$) to 117 cm^{-1} at the Brillouin zone boundary. The top of the optic continuum was taken as the weak IR band at 615 cm^{-1}. The symmetric Si-O-Si stretching frequencies were taken as 6.7% of the total modes and placed at 730 cm^{-1} [*Lazarev*, 1972, p. 103]. These modes probably span a range of frequencies from 670 to 750 cm^{-1}, but no mode assignments have been made for jadeite. The antisymmetric stretching modes were represented by 10% of the modes at 1000 cm^{-1} and 10% at 900 cm^{-1}.

The results of the model are shown in Figure 4, where they are compared with the experimental data of *Kelley et al.* [1953]. The agreement is good except at very low temperatures. The model value of C_V* at 298°K is 3.81 cal mole^{-1} °K^{-1}; the value obtained from experimental data is 3.80 cal mole^{-1} °K^{-1} [*Robie et al.*, 1978, p. 391]. The model value of S_{298}* is 3.30 cal mole^{-1} °K^{-1}; the experimental value is 3.19 cal mole^{-1} °K^{-1}. Acoustic and optic modes contribute about equally to the heat capacity at 40°K. Above this temperature the optic modes dominate the behavior of C_V*.

The main differences in C_V* between jadeite and diopside occur at low temperatures. For example, at 53.8°K the C_V* (measured) of diopside is 13% greater than the C_V of jadeite; at 298°K it is 4% greater. The model predicts a similar relationship and shows that the acoustic mode contributions at low temperatures are nearly identical for the two minerals and that the difference in C_V* is caused by the contribution of the relatively lower frequency optic modes in diopside. These modes are cation-oxygen deformations, and it is consistent with the heavier mass of calcium relative to sodium that these modes occur at lower frequencies in diopside and thus contribute to a higher low-temperature heat capacity.

The complex relations between the heat capacities of jadeite and albite are also explicable in terms of the spectral and, ultimately, structural differences. First, a correction must be made to the model values reported in paper 3: these were erroneously based on a unit cell content of four formula units of $NaAlSi_3O_8$, whereas the primitive unit cell should contain only two formula units. The model parameters and values of C_V* and S* are given in Tables 1 and 3. As was mentioned in paper 3, the number of atoms in the unit cell determines the fraction which are acoustic modes (3/3*s*, where *s* is the number of atoms per unit cell) and hence affects both the acoustic and the optic contribution to the thermodynamic properties.

Returning now to the comparison of jadeite with albite, we can see that the reason that albite has nearly twice the heat capacity per atomic weight (C_V*) as jadeite at low temperatures (<100°K) is that the optic modes of albite extend to much lower frequencies (83 versus 152 cm^{-1} at $\mathbf{K} = \mathbf{0}$; 63 versus 117 cm^{-1} at $\mathbf{K}_{max}$). However, as the temperature rises toward room temperature, the effect of modes in the middle part of the spectrum becomes felt. There are more modes at frequencies between 200 and 500 cm^{-1} for jadeite than for albite and therefore a larger contribution to the heat capacity. Hence at 298°K the heat capacity per atomic mass of jadeite is greater than that of albite. Because the spectra of the two minerals do not differ much at high frequencies, the heat capacities are similar above room temperature.

The lower frequencies of the Na-O vibrations in albite in

comparison with jadeite may be attributable to longer, and therefore weaker, Na-O bonds: six of the Na-O bonds in albite are in the range 2.38–2.86 Å, and two others are 3.12 and 3.45 Å, whereas the Na-O bonds in jadeite are all between 2.357 and 2.741 Å [*Wyckoff*, 1968, p. 297].

The above comparisons of diopside, jadeite, and albite suggest that structural changes cause larger heat capacity variations than chemical (ionic substitution) changes.

Tremolite. The crystallographic structures of tremolite ($Ca_2Mg_5Si_8O_{22}(OH)_2$) and diopside are identical when projected on (010) [*Bragg et al.*, 1965, p. 236]. The difference between the structures is in the arrangement of the atoms in the *b* direction: in tremolite the silicon-oxygen chains are doubled across a plane perpendicular to the *a* direction. Tremolite belongs to the monoclinic *C2/m* space group and therefore has one formula unit (41 atoms) in the primitive unit cell of volume 453.15×10^{-24} cm^3 and has 123 degrees of freedom per unit cell.

Three of these degrees of freedom are acoustic. The acoustic velocities of tremolite were taken as $u_1 = u_2 = 3.70$ km s^{-1} and $u_3 = 6.17$ km s^{-1} [*Woeber et al.*, 1963]. Because of the lack of acoustic data and structural analogues for which acoustic anisotropies are known, shear anisotropy was not included in the model. The mean sound speed is 4.09 km s^{-1}, and the elastic Debye temperature is 547°K, substantially lower than the value for diopside. The acoustic velocities and unit cell parameters give acoustic shear branches which truncate at 64 cm^{-1} and a longitudinal branch at 106 cm^{-1} at the Brillouin zone boundary.

Optical data on tremolite are sparse (a listing of modes by *Liese* [1975, p. 218] and a partial listing and discussion by *Lazarev* [1972, p. 112]). The vibrations associated with the Si_4O_{11} ribbon occur in two regions of the spectrum: a high-frequency band from 900 to 1100 cm^{-1} and a low-frequency band from 645 to 758 cm^{-1}. The antisymmetric Si-O-Si stretching band was subdivided into two parts: an Einstein oscillator at 1050 cm^{-1} containing 8.9% of the modes and one at 950 cm^{-1} containing 8.9%; 8.1% of the modes were placed at 700 cm^{-1}. The O-H stretching modes were taken as constituting 1.6% of the total modes and placed at 3677 cm^{-1}. Under the assumption that the remainder of the vibrational spectrum is similar to that of diopside the low-frequency cutoff of the optic continuum was taken as 150 cm^{-1} in the model (reduced by dispersion to 127 cm^{-1} at the Brillouin zone boundary). The high-frequency cutoff of the optic continuum was taken at 545 cm^{-1}.

The model values of C_V* are given in Figure 4, where they are compared with the experimental values of *Robie and Stout* [1963] from 12° to 305°K. There is a slight difference between the model and experimental values below 50°K, where the experimental values show an unusual behavior (see the $\theta_{cal}(T)$ values in Figure 4*b*), but in general, the agreement is good. The model value of C_V* at 298°K is 3.87 cal mole^{-1} °K^{-1}; the experimental value is 3.81 cal mole^{-1} °K^{-1}. The model value of S_{298}* is 3.38 cal mole^{-1} °K^{-1}; the experimental value is 3.20 cal mole^{-1} °K^{-1}.

The effect of the OH^- stretching modes on the thermodynamic properties of tremolite, talc, and muscovite is best seen in the calorimetric Debye temperature curves in Figure 4*b*. Although these modes constitute only a few percent of the total modes, they cause $\theta_{cal}(T)$ to rise to very high temperatures, because the O-H stretching modes are at very high frequencies. As was demonstrated in paper 1 (equation (39)), the limiting value of $\theta_{cal}(T)$ obtained at high temperatures, designated as $\theta_{cal}(\infty)$, depends on both the frequency of the Einstein mode and the fraction of oscillators associated with it. For most minerals, however, dehydration may take place at temperatures below those at which the OH^- stretching modes contribute significantly to the heat capacity.

Sheet Silicates

Muscovite. Muscovite ($KAl_2(AlSi_3)O_{10}(OH)_2$) is a 2:1 dioctahedral silicate [*Farmer*, 1974*b*, p. 332] in which hexagonal silicate anions are linked together by cations in octahedral coordination, giving a structural unit resembling a sandwich. These units are weakly linked together by interlayer cations. The crystallographic unit cell of muscovite is monoclinic *C2/c*; therefore the primitive unit cell is half of the volume of the crystallographic unit cell ($V_L = 466.65 \times 10^{-24}$ cm^3), and there are 42 atoms per unit cell, giving 126 degrees of freedom per unit cell.

The acoustic properties of muscovite are highly anisotropic [*Alexandrov and Ryzhova*, 1961]; for example, shear velocities vary from 2 to 5 km s^{-1}, and longitudinal velocities vary from 4.5 to 8 km s^{-1}. The VRH shear velocity is 3.53 km s^{-1}, and the VRH longitudinal velocity is 5.78 km s^{-1} [*Simmons and Wang*, 1971, 52640]. The directionally averaged shear velocities used in the model are $u_1 = 3.21$ and $u_2 = 4.02$ km s^{-1}. The mean sound speed is $v_m = 3.90$ km s^{-1}, and the elastic Debye temperature is 520°K.

The lattice vibrations of layer silicates can approximately be separated into the vibrations of the hydroxyl groups, the silicate anions, the octahedral cations, and the interlayer cations [*Farmer*, 1974*b*, p. 331]. Three groups of vibrations are quite well separated in frequency. The O-H stretching vibrations are in the region 3400–3750 cm^{-1}, the Si-O stretching vibrations are in the range 690–1200 cm^{-1}, and the interlayer cation vibrations are between ~100 and 150 cm^{-1}. The remaining vibrations are less well isolated, but their general classification is still useful: OH librational vibrations lie in the region 600–950 cm^{-1} (overlapping the (Si, Al)-O stretching frequencies), and the Si-O bending vibrations lie between 150 and 600 cm^{-1}. These latter vibrations are strongly coupled with vibrations of the octahedral cations and with the translatory vibrations of the hydroxyl groups [*Farmer*, 1974*b*, p. 331].

The lowest optical mode of muscovite was taken at 108 cm^{-1} (reduced to 91 cm^{-1} by dispersion across the Brillouin zone). This is the wave number of the in-plane vibration of K^+ [*Farmer*, 1974*b*, p. 351]. As was discussed in section 1, the choice of the top of the optic continuum is complicated by the overlap of a number of modes. I chose 620 cm^{-1} as the top of the optic continuum, assigning higher modes to two classes of Si-O vibrations: 15.9% at 1000 cm^{-1} for the averaged frequency of the high-frequency (Si, Al)-O-Si modes which extend from 900 to 1100 cm^{-1} and 9.5% at 800 cm^{-1} to represent the lower-frequency symmetric stretching modes. The OH stretching modes were represented by an Einstein oscillator at 3633 cm^{-1} containing 3.2% of the modes.

The results of the model are shown in Figure 4, where they are compared with the calorimetric data of *Robie et al.* [1976] from 15° to 375°K. The excellent agreement of the model with the data even to very low temperatures suggests that the model spectrum is a reasonable approximation to the real lattice vibrational spectrum and, in particular, that there are not a significant number of lattice modes below the value of 91

cm^{-1} used in the model. The model value of C_V^* at 298°K is 3.68 cal $mole^{-1}$ $°K^{-1}$; the experimental value is 3.70 cal $mole^{-1}$ $°K^{-1}$. The model value of S_{298}^* is 3.31 cal $mole^{-1}$ $°K^{-1}$; the experimental value is 3.27 cal $mole^{-1}$ $°K^{-1}$. A configurational entropy S_{ci}^* of 0.223 cal $mole^{-1}$ $°K^{-1}$ should be added to the measured or calculated harmonic and anharmonic contributions of the real (disordered) muscovite [*Ulbrich and Waldbaum,* 1976, p. 10; *Robie et al.,* 1976, p. 643]. At 30°K, optic modes contribute 50% of the heat capacity. The contribution of Si-O stretching modes is significant by room temperature, but the O-H stretching modes do not contribute to C_V^* appreciably over the range of temperatures considered.

Talc. Talc ($Mg_3(Si_4O_{10})(OH)_2$) is a trioctahedral 2:1 layer silicate [*Farmer,* 1974*b*, p. 332]. The sandwich units formed by the silicate anions are weakly linked by van der Waals forces. Talc is monoclinic with space group $C2/c$; therefore the primitive unit cell contains half the contents of the crystallographic unit cell: 42 atoms in a volume $V_L = 452 \times 10^{-24}$ cm^3.

Although acoustic and spectral data on talc are limited, I attempted a model for comparison with muscovite, tremolite, and enstatite because excellent low-temperature calorimetric data have been published [*Robie and Stout,* 1963]. Only a few of the directional acoustic velocities of talc have been measured [*Alexandrov and Ryzhova,* 1961]. The published velocities are similar to the values for muscovite, and because VRH average values for talc have not been calculated, the muscovite values were used for this study. These velocities give a mean sound speed of 3.90 km s^{-1} and, in conjunction with the unit cell parameters and density of talc, give an elastic Debye temperature of 525°K.

Spectral data on talc are also limited, and interpretations of mode frequencies found in the literature are somewhat confusing. The lowest observed spectral bands are at 160–190 cm^{-1} [*Ishii et al.,* 1967]. However, predicted values (based on simple force constant models) are as low as 80 cm^{-1}. The observed value of 170 cm^{-1} was used as the lower cutoff of the optic continuum in the model; it is lowered to 132 cm^{-1} by dispersion across the Brillouin zone. The upper limit of the optic continuum was taken to be 620 cm^{-1}, the same value as for muscovite; this band does not appear in the infrared spectrum shown by *Farmer* [1974*b*, p. 344] but is given as the calculated frequency of the a_1^2 mode of an ideal hexagonal $(Si_2O_5)_n$ layer. The Si-O stretching modes were represented by 15.9% of the modes at 1000 cm^{-1} and 9.5% at 800 cm^{-1}.

Model values of C_V^* are given in Figure 4, where they are compared with the experimental values of *Robie and Stout* [1963] from 12° to 305°K. Given the uncertainties in the data, the agreement is surprisingly good. The model value of C_V^* at 298°K is 3.61 cal $mole^{-1}$ $°K^{-1}$; the experimental value is 3.65 cal $mole^{-1}$ $°K^{-1}$. The model value of S_{298}^* is 2.99 cal $mole^{-1}$ $°K^{-1}$; the experimental value is 2.97 cal $mole^{-1}$ $°K^{-1}$.

A comparison of the talc and muscovite heat capacities and spectra shows that the higher heat capacity of muscovite arises from the lower-frequency cation-oxygen modes in the vicinity of 100 cm^{-1}.

5. Model Values of the Temperature Dependence of C_V^* and S^* for 32 Minerals

This model provides an internally consistent method for calculation of the thermodynamic functions of a mineral from elastic, crystallographic, and spectroscopic data. It should be particularly useful for examining these functions in temperature ranges where experimental data have not been obtained (e.g., $T < 54$°K for many minerals) and at temperatures where minerals are unstable (such as above 300°K for stishovite and coesite). The harmonic contributions to the heat capacity at constant volume, C_V^*, the internal energy E^*, the Helmholz energy F^*, and the entropy S^* can be easily calculated from the expressions given in Tables 1 and 2 of paper 1. The values of C_V^* and S^* at three temperatures are given in Table 3. In a few cases the model parameters have been changed from those used in paper 3 where new data or interpretations have become available (for example, I have now consistently attempted to define the Si-O stretching modes more precisely than in paper 3, because these modes make large contributions to the zero-point energy and are important in the isotopic fractionation calculation discussed in paper 5). The parameters used for the tabulated values are given in Table 1. The model values are compared with experimental values obtained from *Robie et al.* [1978] except where noted.

In order to compare the calculated C_V^* with the experimentally measured quantity C_P^* an anharmonic correction must be added; the method used for this is described in Appendix B. At the high temperatures 700° and 1000°K this contribution is significant. It is not well determined, because the thermal expansion of many minerals is poorly known. Therefore differences of 5% between the model values and the experimental values at high temperatures may reflect uncertainties in this term rather than differences caused by spectral properties.

6. Summary and Comments on the Accuracy of the Model

With this paper the calculation of thermodynamic properties for minerals is completed; 32 minerals have been examined, and the thermodynamic functions have been calculated from elastic, crystallographic, and spectroscopic data alone. The purpose has been to demonstrate that the functions can indeed be predicted to an accuracy sufficient to allow problems of geologic and geophysical interest to be solved. The accuracy of the model for a given mineral depends on (1) the degree to which the real lattice vibrational spectrum is approximated by the simple model spectrum and (2) the quantity and quality of acoustic and spectral data available. As was discussed in section 6 of paper 3, the model has different accuracies in different temperature ranges: for C_V^*, typically ±30–50% below 50°K, ±5% at 298°K, and ±1% at 700°K. In order to give the reader an idea of the overall accuracy which might be expected, I have compared the model entropies at 298.15°K with calorimetrically determined entropies of the minerals. Entropy was chosen for comparison of measured and calculated values because it is the thermodynamic quantity most sensitive to the assumed frequency distribution (other than the very low temperature heat capacity). The reason for the sensitivity is shown in Figure 5. Because the entropy S^* is the integrated value of C_P^*/T, it is dominated by the contributions of the low-frequency modes, and because the model is weakest in its representation of the low-frequency part of the optic continuum, the entropy reflects, in effect, the weakest aspects of the model. Note from Figure 5 that the heat capacity below about 50°K does not strongly affect the entropy at 298°K, so that the large uncertainties in the heat capacity at very low temperatures do not strongly affect the entropy at 298°K.

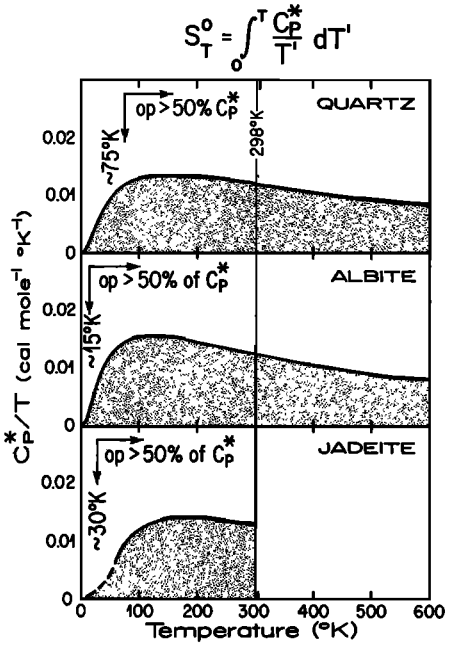

Fig. 5. C_P^*/T versus T for quartz, albite, and jadeite. The third-law entropies are simply the areas under the curves. The temperatures at which optical modes contribute more than 50% of the heat capacity are shown with orthogonal arrows, and it can be seen that the entropy at high temperatures is dominated by the contributions of the optic modes. It can also be seen that only a small fraction of the 298°K entropy arises below 50°K and that the behavior of C_P^*/T in the range 100°–200°K determines a large part of the 298°K entropy.

The comparison of model and experimental entropies is given in Table 3. Minerals for which low-temperature calorimetry is available and for which there is little question that the data represent the harmonic heat capacity without complications due to magnetic or electronic contributions, phase changes, or metastability of phases are shown in boldface. *Openshaw* [1974, p. 143] has demonstrated that significant errors in $S_{298.15}$ may exist if entropies are calculated from heat capacity data which extend only down to 54°K—errors of the order of 1–1.5 cal mole^{-1} °K^{-1} in the molar entropy, that is, a few percent. Therefore for the comparison of model values of S_{298} with measured values, only well-determined values are used. For the 14 minerals indicated, the average value of the absolute values of the deviations of the model from the measured values is 1.5%.

For most of the minerals for which the deviation of the model from the experimental values is large (including those for which experimental data go only to 50°K) an explanation for the discrepancy can be proposed as follows:

Brucite. The acoustic velocities used in the model were estimated from shock wave data (see paper 3) and are therefore quite uncertain. The acoustic modes calculated from these velocities contribute more heat capacity at 50°K (C_V^* = 0.346 cal mole^{-1} °K^{-1}) than the total measured heat capacity at that temperature (C_V^* = 0.232 cal mole^{-1} °K^{-1}). Therefore the acoustic velocities used are probably in error (underestimated).

Silica glass, coesite. Plausible spectral models bracket the measured thermodynamic properties. In the case of glass, validity of the application of the model itself may be questioned, as was discussed in paper 3; in the case of coesite, Raman data and spectral interpretations are needed.

Stishovite. The model greatly overestimates the low-temperature heat capacity and therefore the 298°K entropy. The cause of the discrepancy cannot be given. Calorimetric data and spectral data both present problems, as discussed in papers 2 and 3, but none of the problems discussed would resolve this discrepancy. A critical examination of the relations between the structure of stishovite and its spectral and calorimetric data should be considered.

Tremolite. The model was based on very little spectral data and use of an analogy to diopside. Far-infrared and Raman data are needed.

In conclusion, the proposed model is much more accurate than the Debye model for calculation of the thermodynamic functions and provides a way to estimate or extrapolate these functions with sufficient accuracy to allow problems of geologic interest to be addressed. A method for using the model to supplement partial calorimetric data is given in Appendix A.

APPENDIX A: A METHOD FOR COMBINING THE MODEL WITH CALORIMETRIC DATA

The model demonstrates that the heat capacities of minerals are very sensitive to the distribution of optic modes at low frequencies. This limits the accuracy obtainable from the model, because even when both infrared and Raman spectral data are available, the spatially averaged distribution of frequencies is not known. Because no adequate models exist for extrapolating the behavior of the modes at $\mathbf{K} = \mathbf{0}$ across the Brillouin zone to $\mathbf{K} = \mathbf{K}_{max}$, the parameter w_l is not well defined from existing data. A marked improvement can be made in the overall accuracy of the calculations of the calorimetric functions if the parameter w_l is obtained by fitting to measured calorimetric data in the range 50°–300°K. With such a procedure, illustrated below, accurate extrapolation of existing data to low temperatures should be possible. The frequency w_l so obtained then becomes a parameter rather than the Brillouin zone boundary frequency defined in the previous papers of this series. The parameter thus obtained may be more meaningful as a directionally averaged mode frequency than is the parameter obtained from spectroscopic data at $\mathbf{K} = \mathbf{0}$ and extrapolated from $\mathbf{K} = \mathbf{0}$ to $\mathbf{K} = \mathbf{K}_{max}$ across the Brillouin zone by the simple scheme adopted in these papers.

In order to choose the temperature at which the heat capacities are most sensitive to the parameter w_l, and thereby to select the best temperatures for fitting this parameter, consider Figure 5. At very low temperatures (below 15°–75°K, depending on the mineral considered) the thermodynamic functions depend primarily on the acoustic modes and therefore are relatively independent of w_l. At higher temperatures (above approximately 200°K) the thermodynamic functions are too insensitive to details of the optic continuum to provide a sensitive measure of w_l, because the low-frequency modes are saturated and contribute uniformly to the thermodynamic functions. In the range 50°–200°K the thermodynamic functions are most sensitive to the low-frequency distribution of optic modes. Study of Figure 5 suggests that fitting at about 100°K will optimize prediction of the entropy, because the largest contribution per unit temperature change occurs in this range; experience with the model has shown that this is a better temperature to use than the lowest temperature, 54°K, at which calorimetric data have often been obtained.

The procedure for obtaining w_l will now be described for tremolite, a mineral for which so few spectral data were avail-

TABLE B1. Values of Parameters in $C_P^* - C_V^*$ Correction

Mineral	V_0,[a] cm^3 mole^{-1}	ϵ_0,[b] °K^{-1} × 10^6	ϵ_1,[b] °K^{-2} × 10^6	ϵ_2, °K^{-3} × 10^{12}	B_0,[c] Mbar	$\partial B_0/\partial T$,[d] Mbar °K^{-1} × 10^3
			Simple Minerals			
Halite	27.018	69.792	0.144		0.240	
Periclase	11.250	25.884	0.021		1.631	−0.210
Brucite	24.640	19.288[e]	0.013		0.710	
Corundum	25.570	11.522	0.021		2.537	−0.230
Spinel	39.720	18.485	0.013	−2.34	1.930	−0.210
			Framework Minerals			
α-Quartz	22.700	−32.176[f]	0.173		0.377	−0.100
α-Cristobalite	25.740	71.814[g]	0.076		0.374	
		61.447[h]	−0.063		0.374	
Coesite	20.640	5.770	0.008		1.139	
Silica glass	27.270	1.620			0.372	
Stishovite	14.016	20.250[i]	0.009	−0.500	3.333	
Rutile	18.800	20.250	0.009	−0.500	2.130	
Albite	100.210	12.955	0.019		0.576	
Microcline	108.690	1.094	0.021		0.547	
Anorthite	100.210	7.638	0.010		0.495	
			Sheet and Chain Minerals			
Talc	136.700	19.288[e]	0.013		0.468	
Muscovite	140.550	19.288[e]	0.013		0.475	
Tremolite	272.950	19.288[e]	0.013		0.587	
Enstatite	31.470	22.031	0.010		0.996	
Jadeite	60.980	13.319	0.023		1.214	
Diopside	66.100	21.031	0.010		1.094	
			Orthosilicates			
Forsterite	43.798	17.969	0.026		1.345	−0.210
Zircon	39.270	6.252	0.011		2.059	
Pyrope	113.290	15.439	0.014		1.647	−0.220
Grossular	125.320	14.288	0.013		1.692	
Spessartine	118.160	9.166	0.024		1.711	
Almandine	115.280	10.303	0.019		1.792	−0.230
Andradite	131.670	18.031	0.010		1.473	
Kyanite	44.110	6.559	0.024		2.645	
Andalusite	51.540	7.893	0.035		1.731	
Sillimanite	49.910	4.061	0.021		1.835	
Calcite	36.940	4.285	0.030		0.777	

Where there is no entry, the value is assumed to be zero.

[a] All molar volumes are from *Robie et al.* [1966, Table 5-2].

[b] The volume thermal expansion coefficients ϵ_0 and ϵ_1 were obtained from least squares fit of three data points from *Skinner* [1966] except for periclase and calcite, for which data from *Touloukian and Ho* [1977] were used. For minerals for which data were not available, estimates from analogues were used, as indicated in these footnotes.

[c] Values of the bulk modulus were calculated from values of v_s and v_p given in these papers, ϵ listed in this table, and ρ and C_p from the tables for equations (1), (4), (5), (10), and (13) of *O. L. Anderson et al.* [1968]. The calculations were done by J. M. Delany.

[d] Values of the bulk modulus derivative with respect to temperature were obtained from *O. L. Anderson et al.* [1968].

[e] Hornblende values are used for ϵ_0, ϵ_1, and ϵ_2.

[f] This value was used only for an estimate of the anharmonic terms. Tabulated values of C_V from *Lord and Morrow* [1957] were used in the paper.

[g] $T < 491$°K.

[h] $T > 491$°K.

[i] Values for rutile were used.

able that the model discussed in the text was based on data from diopside. Assume first that the measured C_P^* at 100°K of 1.144 cal mole^{-1} °K^{-1} is equal to C_V^*. First calculate the contribution of the acoustic modes at this temperature. For the primitive unit cell of tremolite there are 123 degrees of freedom, three of which are acoustic. Using Table 1 of paper 3, we find that these modes contribute 0.1332 cal mole^{-1} °K^{-1} at 100°K. (As a first approximation these modes are nearly saturated at 100°K.) There are four Einstein oscillators in the model: one at 1050 cm^{-1} containing 8.9% of the modes, one at 950 cm^{-1} containing 8.9% of the modes, one at 700 cm^{-1} containing 8.1% of the modes, and one at 3677 cm^{-1} containing 1.6% of the modes. At 100°K these four Einstein oscillators contribute 0.0022 cal mole^{-1} °K^{-1} to the heat capacity (i.e., approximately zero). Therefore 1.144 − 0.1332 − 0.0022 = 1.0086 cal mole^{-1} °K^{-1} is to be contributed by the optic continuum. This continuum contains $(1 - 1/s - q_1 - q_2 - q_3 - q_4)$ = 0.7006 of the modes. The upper cutoff frequency of the continuum is taken as 545 cm^{-1}, so that x_u (the nondimensionalized frequency defined in paper 3) is 545 × 1.44/

100 = 7.848. We therefore seek, from Table 2 of paper 3, the value of x_l that gives

$$1.0086 = 3N_A k(1 - 1/s - q_1 - q_2 - q_3 - q_4)\mathscr{K}\begin{pmatrix} x_u \\ x_l \end{pmatrix}$$

or

$$\mathscr{K}\begin{pmatrix} 7.848 \\ x_l \end{pmatrix} = 0.2415$$

The value is $x_l = 2.1$, for which $w_l = 146$ cm^{-1}. This represents the lowest limit of the optic continuum and is to be compared with the zone boundary frequency calculated by the dispersion relation discussed in the text. For tremolite this value was 127 cm^{-1}, obtained from the $\mathbf{K} = \mathbf{0}$ mode frequency of 150 cm^{-1}. The new value of 146 cm^{-1} would correspond to a zone center frequency of 172 cm^{-1} if the same behavior were assumed.

The heat capacity C_V^* at 298°K with this model is 3.83 cal mole^{-1} °K^{-1}; the entropy S^* is 3.22 cal mole^{-1} °K^{-1}. The error in the calculated entropy at 298°K has decreased from 5.6 to 0.6%.

Appendix B: Estimate of the $C_P^* - C_V^*$ Correction and the Anharmonic Entropy

The correction from C_V^* to C_P^* is given by

$$C_P^* - C_V^* = TV\epsilon^2 B$$

where T is the temperature, V is the molar volume

$$V \approx V_0 + (\partial V/\partial T)\Delta T$$

ϵ is the thermal expansion

$$\epsilon = \epsilon_0 + \epsilon_1 T + \epsilon_2 T^2 + \epsilon_3 T^3 + \cdots$$

and B is the bulk modulus

$$B \approx B_0 + (\partial B/\partial T)\Delta T$$

In these equations, V_0, ϵ_0, and B_0 are the parameters at a reference temperature, and ΔT is the difference between the temperature of the calculation and the reference temperature. For V and B the reference temperature is 298°K; for ϵ it is 0°K, because the coefficients ϵ_0, ϵ_1, and ϵ_2 were obtained by least squares fitting of three or more data points with respect to absolute temperature (see Table B1). As can be seen from Table 3, at 298°K the $C_P^* - C_V^*$ correction is of the order of 1%, the largest correction being for halite, 5%.

The entropy is obtained by integration:

$$S^* = \int_0^{T_f} (C_P^*/T)\,dT = \int_0^{T_f} (C_V^*/T)\,dT + \int_0^{T_f} V\epsilon^2 B\,dT$$

where $\int_0^{T_f} (C_P^*/T)\,dT$ is referred to in this paper as the 'total entropy,' $\int_0^{T_f} (C_V^*/T)\,dT$ is referred to as the 'harmonic entropy,' and $\int_0^{T_f} V\epsilon^2 B\,dT$ is referred to as the 'anharmonic entropy.' If V, ϵ, and B were independent of temperature, then the anharmonic entropy would be given by $TV\epsilon^2 B$; that is, it would be the same as the heat capacity correction. Because V, B, and ϵ are functions of temperature, as given above, this integral should be evaluated by proper integration of the products of the temperature-dependent functions. For all practical purposes, V and B are independent of temperature, because $\partial B/\partial T$ and $\partial V/\partial T$ provide very small changes over the range of temperatures considered. Therefore to a good approximation,

$$\int_0^{T_f} V\epsilon^2 B\,dT \approx \int_0^{T_f} V_0 B_0(\epsilon_0^2 + 2\epsilon_0\epsilon_1 T + \epsilon_1^2 T^2 + \cdots)\,dT$$

(where the terms containing ϵ_2 are dropped from the explicit notation, because this coefficient was generally assumed to be zero). When integrated, the second and third terms contribute about a 25% correction to the first term at 300°K and approximately double the contribution of the first term at 1000°K (assuming that $\epsilon_0 \approx 20 \times 10^{-6}$ and $\epsilon_1 \approx 2 \times 10^{-8}$). Because the estimate of $\epsilon(T)$ is relatively simplistic and because the anharmonic contribution to S^* is of the order of 1% at 300°K, I have used the approximation $S_{an}^* \approx TV\epsilon^2 B$ in Table 3. The reader is cautioned that if an estimate of total entropy at 300°K is required to be accurate to within 1–3% or if an estimate of the total entropy at higher temperatures is required, the anharmonic contribution should be calculated carefully with a good model for $\epsilon(T)$; the values given in Table 3 for this correction are probably minimum values of S_{an}^*.

Appendix C: Corrections to Papers 1–3

Paper 1

In Table 1, in the expressions for the Helmholtz free energy F the term $3nN_A\beta$ should be preceded by a minus sign.

Equation (15) should read

$$C_V = \frac{12\pi^4}{5} nN_A k\left(\frac{T}{\theta_D}\right)^3$$

Paper 2

In Table 3 the lowest optic mode for enstatite should be ~110 instead of 140 cm^{-1}.

Paper 3

In Table 5, for spinel, $q = 0.19$, as in Figure 2.

Model values for albite were based erroneously on a unit cell content of four formula units instead of two (see paper 3, p. 55). See the discussion in section 4 of this paper, in the subsection on jadeite.

The value of $w_l(\mathbf{K} = \mathbf{0})$ for spinel (Tables 4 and 5 and p. 49) has been changed from 225 to 311 cm^{-1}, based on a reevaluation of the data (see paper 4, Table 1).

Notation

The reader is referred to the notation lists at the ends of papers 1–3. Additional symbols used in this paper are as follows.

ϵ thermal expansion.

$\epsilon_0, \epsilon_1, \epsilon_2, \cdots$ coefficients in polynomial series of thermal expansion.

Acknowledgments. The author thanks J. Delany, E. Essene, R. A. Robie, R. R. Reeber, and D. F. Westrum, Jr., for reviewing the manuscript.

References

Alexandrov, K. S., and T. V. Ryzhova, Elastic properties of rock-forming minerals, II, Layered silicates (in Russian), *Izv. Akad. Nauk. SSSR, Ser. Geofiz.*, no. 12, 1799–1804, 1961. (*Bull. Acad. Sci. USSR, Geophys. Ser.*, Engl. Transl., no. 12, 1165–1168, 1971.)

Althaus, E., The triple point andalusite-sillimanite-kyanite, *Contrib. Mineral. Petrol., 16,* 29–44, 1967.

Anderson, C. T., The heat capacities at low temperatures of the alkaline earth carbonates, *J. Amer. Chem. Soc., 56,* 340–342, 1934.

Anderson, O. L., The determination and some uses of isotropic elastic constants of polycrystalline aggregates using single-crystal data, in *Physical Acoustics,* vol. IIIB, edited by W. P. Mason, p. 43, Academic, New York, 1965.

Anderson, O. L., and R. C. Liebermann, Sound velocities in rocks and minerals, *Contract Rep. 7885-4-X,* Willow Run Lab., Ann Arbor, Mich., 1966.

Anderson, O. L., E. Schreiber, R. C. Liebermann, and N. Soga, Some elastic constant data on minerals relevant to geophysics, *Rev. Geophys. Space Phys., 6,* 491–524, 1968.

Babushka, V., J. Ficila, M. Kumazarva, I. Ohno, and Y. Sumino, Elastic properties of garnet solid-solution series, *Phys. Earth Planet. Interiors, 16,* 157–176, 1978.

Bhimasenachar, J., and G. Venkataratnam, Elastic constants of zircon, *J. Acoust. Soc. Amer., 27,* 922–925, 1955.

Bonczar, L. J., E. K. Graham, and H. Wang, The pressure and temperature dependence of the elastic constants of pyrope garnet, *J. Geophys. Res., 82,* 2529–2534, 1977.

Bottinga, Y., Calculation of fractionation factors for carbon and oxygen isotopic exchange in the system calcite–carbon dioxide–water, *J. Phys. Chem., 72,* 800–808, 1968.

Bragg, L., G. F. Claringbull, and W. H. Taylor, *Crystal Structures of Minerals,* vol. IV of *The Crystalline State,* edited by L. Bragg, 409 pp., Cornell University Press, Ithaca, N. Y., 1965.

Cantor, S., Entropy estimates of garnets and other silicates, *Science, 198,* 206–207, 1977.

Cowley, E. R., and A. K. Pant, Lattice dynamics of calcite, *Phys. Rev. B, 8,* 4795–4800, 1973.

Dawson, P., M. M. Hargreave, and G. R. Wilkinson, The vibrational spectrum of zircon, *J. Phys. C, 4,* 240–256, 1971.

Farmer, V. C., Orthosilicates, pyrosilicates and other finite chain silicates, in *The Infrared Spectra of Minerals, Monogr. 4,* edited by V. C. Farmer, pp. 285–303, Mineralogical Society, London, 1974*a*.

Farmer, V. C., The layer silicates, in *The Infrared Spectra of Minerals, Monogr. 4,* edited by V. C. Farmer, pp. 331–363, Mineralogical Society, London, 1974*b*.

Gibbs, G. V., and J. V. Smith, Refinement of the crystal structure of synthetic pyrope, *Amer. Mineral., 50,* 2023–2039, 1965.

Goto, T., I. Ohno, and Y. Sumino, The determination of the elastic constants of natural almandine-pyrope garnet by rectangular parallelepiped resonance method, *J. Phys. Earth, 24,* 149–156, 1976.

Haselton, H. T., and E. F. Westrum, Jr., Heat capacities (5–350 K) of synthetic pyrope, grossular, and pyrope 60, grossular 40 (abstract), *Eos Trans. AGU, 60,* 405, 1979.

Haselton, H. T., and E. F. Westrum, Jr., Low-temperature heat capacities of synthetic pyrope, grossular, and pyrope 60 grossular 40, *Geochim. Cosmochim. Acta, 44,* 701–709, 1980.

Hearmon, R. F. S., The elastic constants of anisotropic material, *Advan. Phys., 5,* 323–382, 1956.

Herzberg, G., *Infra-Red and Raman Spectra of Polyatomic Molecules,* 632 pp., Van Nostrand, New York, 1945.

Holdaway, M. J., Stability of andalusite and the aluminum silicate phase diagram, *Amer. J. Sci., 271,* 97–131, 1971.

Holm, J. L., and O. J. Kleppa, The thermodynamic properties of aluminum silicates, *Amer. Mineral., 51,* 1608–1622, 1966.

Horai, K., and G. Simmons, An empirical relationship between thermal conductivity and Debye temperature for silicates, *J. Geophys. Res., 75,* 978–982, 1970.

Isaak, D. G., and E. K. Graham, The elastic properties of an almandine-spessartine garnet and elasticity in the garnet solid solution series, *J. Geophys. Res., 81,* 2483–2489, 1976.

Iishi, K., Lattice dynamics of forsterite, *Amer. Mineral., 63,* 1198–1208, 1978.

Iishi, K., E. Salje, and C. L. Werneke, Phonon spectra and rigid-ion model calculations on andalusite, *Phys. Chem. Miner., 4,* 173–188, 1979.

Ishii, M., T. Shimanouchi, and M. Nakahira, Far infrared absorption spectra of layer silicates, *Inorg. Chim. Acta, 1,* 387–392, 1967.

Janaf (Joint Army, Navy, and Air Force Project Principia of the Advanced Research Projects Agency), Thermochemical tables, 2nd ed., Nat. Stand. Ref. Data Ser., vol. 37, 1141 pp., Nat. Bur. of Stand. Washington, D. C., 1965*a*. (Also available as catalog C 13.48:37 from Clearinghouse, U.S. Dep. of Commer., Springfield, Va.)

Janaf (Joint Army, Navy, and Air Force Project Principia of the Advanced Research Projects Agency), Thermochemical tables, first addendum, Therm. Res. Lab., Dow Chem. Co., Midland, Mich., 1965*b*.

Janaf (Joint Army, Navy, and Air Force Project Principia of the Advanced Research Projects Agency), Thermochemical tables, second addendum, Therm. Res. Lab., Dow Chem. Co., Midland, Mich., 1966.

Janaf (Joint Army, Navy, and Air Force Project Principia of the Advanced Research Projects Agency), Thermochemical tables, third addendum, Therm. Res. Lab., Dow Chem. Co., Midland, Mich., 1967.

Kelley, K. K., The specific heats at low temperatures of ferrous silicate, manganous silicate and zirconium silicate, *J. Amer. Chem. Soc., 63,* 2750–2752, 1941.

Kelley, K. K., Specific heats at low temperatures of magnesium orthosilicate and magnesium metasilicate, *J. Amer. Chem. Soc., 65,* 339–341, 1943.

Kelley, K. K., S. S. Todd, R. L. Orr, E. G. King, and K. R. Bonnickson, Thermal properties of sodium-aluminum and potassium-aluminum silicates, *U.S. Bur. Mines Rep. Invest., 4955,* 1953.

Kieffer, S. W., Thermodynamics and lattice vibrations of minerals, 1, Mineral heat capacities and their relationships to simple lattice vibrational models, *Rev. Geophys. Space Phys., 17,* 1–19, 1979*a*.

Kieffer, S. W., Thermodynamics and lattice vibrations of minerals, 2, Vibrational characteristics of silicates, *Rev. Geophys. Space Phys., 17,* 20–34, 1979*b*.

Kieffer, S. W., Thermodynamics and lattice vibrations of minerals, 3, Lattice dynamics and an approximation for minerals with application to simple substances and framework silicates, *Rev. Geophys. Space Phys., 17,* 35–59, 1979*c*.

Kieffer, S. W., Thermodynamics and lattice vibrations of minerals, 5, Applications, submitted to *Rev. Geophys. Space Phys.,* 1980.

King, E. G., Low temperature heat capacities and entropies at 298.15 K of some crystalline silicates containing calcium, *J. Amer. Chem. Soc., 79,* 5437–5438, 1957.

Kiseleva, I. A., N. D. Topor, and L. V. Mel'chakova, Experimental determination of heat content and heat capacity of grossularite, andradite and pyrope (in Russian), *Geokhimiya,* no. 11, 1372–1379, 1972.

Kolesnik, Yu. N., V. V. Nogteva, and I. E. Paukov, Heat capacity of pyrope within the temperature range 13–300 K: Thermodynamic properties of some natural garnets (in Russian), *Geokhimiya,* no. 4, 533, 1977.

Kovach, J. J., A. L. Hiser, and C. Karr, Jr., Far-infrared spectroscopy of minerals, in *Infrared and Raman Spectroscopy of Lunar and Terrestrial Minerals,* edited by C. Karr, Jr., pp. 231–254, Academic, New York, 1975.

Krupka, K. M., D. M. Kerrick, and R. A. Robie, Heat capacities of synthetic orthoenstatite and natural anthophyllite from 5 to 1000 K (abstract), *Eos Trans. AGU, 60,* 405, 1979*a*.

Krupka, K. M., R. A. Robie, and B. S. Hemingway, High temperature heat capacities of corundum, periclase, anorthite, $CaAl_2Si_2O_8$ glass, muscovite, pyrophyllite, $KAlSi_3O_8$ glass, grossular, and $NaAlSi_3O_8$ glass between 350 and 1000 K, *Amer. Mineral., 64,* 86–101, 1979*b*.

Kumazawa, M., and O. L. Anderson, Elastic moduli, pressure derivatives, and temperature derivatives of single-crystal olivine and single-crystal forsterite, *J. Geophys. Res., 74,* 5961–5972, 1969.

Lane, D. L., and J. Ganguly, Reevaluation of Al_2O_3 solubility in orthopyroxene in the garnet and spinel fields, and the entropy of pyrope, *Geol. Soc. Amer. Abstr. Programs, 11,* 462, 1979.

Lazarev, A. N., *Vibrational Spectra and Structure of Silicates,* translated from Russian, 302 pp., Consultants Bureau, New York, 1972.

Liese, H. C., Selected terrestrial minerals and their infrared absorption spectral data (4000–300 cm^{-1}), in *Infrared and Raman Spectroscopy of Lunar and Terrestrial Minerals,* edited by Clarence Karr, Jr., pp. 197–229, Academic, New York, 1975.

Lord, R. C., and J. C. Morrow, Calculation of the heat capacity of α-quartz and vitreous silica from spectroscopic data, *J. Chem. Phys., 26,* 230–232, 1957.

Meagher, E. P., The crystal structure of pyrope and grossularite at elevated temperatures, *Amer. Mineral., 60,* 218–228, 1975.

Moore, R. K., W. B. White, and T. V. Long, Vibrational spectra of the common silicates, I, The garnets, *Amer. Mineral., 56,* 54–71, 1971.

Newton, R. C., A. B. Thompson, and K. M. Krupka, Heat capacity of

synthetic $Mg_3Al_2Si_3O_{12}$ from 350 to 1000 K and the entropy of pyrope, *Eos Trans. AGU, 58,* 523, 1977.

Obata, M., The solubility of Al_2O_3 in orthopyroxenes in spinel and plagioclase peridotites and in spinel pyroxenite, *Amer. Mineral., 61,* 804, 1976.

Oehler, O., and H. H. Günthard, Low-temperature infrared spectra between 1200 and 20 cm^{-1} and normal-coordinate analysis of silicates with olivine structure, *J. Chem. Phys., 51,* 4719–4728, 1969.

O'Horo, M. P., A. L. Frisillo, and W. B. White, Lattice vibrations of $MgAl_2O_4$ spinel, *J. Phys. Chem. Solids, 34,* 23–28, 1973.

Omori, K., Analysis of the infrared absorption spectrum of almandine-pyrope garnet from Nijosan, Osaka Prefecture, Japan, *Amer. Mineral., 56,* 841–849, 1971*a*.

Omori, K., Analysis of the infrared absorption spectrum of diopside, *Amer. Mineral., 56,* 1607–1616, 1971*b*.

Openshaw, R., The low temperature heat capacities of analbite, low albite, microcline and sanidine, Ph.D. thesis, 312 pp., Princeton Univ., Princeton, N. J., 1974.

Paques-Ledent, M. T., and P. Tarte, Vibrational studies of olivine-type compounds, I, The i.r. and Raman spectra of the isotopic species of Mg_2SiO_4, *Spectrochim. Acta, Part A, 29,* 1007–1016, 1973.

Peselnick, L., and R. A. Robie, Elastic constants of calcite, *J. Appl. Phys., 34,* 2494–2495, 1963.

Preudhomme, J., and P. Tarte, Infrared studies of spinels, III, The normal II-III spinels, *Spectrochim. Acta, Part A, 27,* 1817–1835, 1971.

Richardson, S. W., M. C. Gilbert, and P. M. Bell, Experimental determination of kyanite-andalusite and andalusite-sillimanite equilibria: The aluminum silicate triple point, *Amer. J. Sci., 267,* 259–262, 1969.

Robie, R. A., and J. L. Edwards, Some Debye temperatures from single-crystal elastic constant data, *J. Appl. Phys., 37,* 2659–2663, 1966.

Robie, R. A., and J. W. Stout, Heat capacity from 12 to 305 K and entropy of talc and tremolite, *J. Phys. Chem., 67,* 2252, 1963.

Robie, R. A., and D. R. Waldbaum, Thermodynamic properties of minerals and related substances at 298.15 K (25.0 C) and one atmosphere (1.013 bars) pressure and higher temperatures, *U.S. Geol. Surv. Bull., 1259,* 256 pp., 1968.

Robie, R. A., P. M. Bethke, M. S. Toulmin, and J. L. Edwards, X-ray crystallographic data, densities and molar volumes of minerals, in *Handbook of Physical Constants, Mem. 97,* edited by S. P. Clark, Jr., pp. 27–73, Geological Society of America, Boulder, Colo., 1966.

Robie, R. A., B. S. Hemingway, and W. H. Wilson, The heat capacities of calorimetry conference copper and of muscovite $KAl_2(AlSi_3)O_{10}(OH)_2$, pyrophyllite $Al_2Si_4O_{10}(OH)_2$, and illite $K_3(Al_7Mg)(Si_{14}Al_2)O_{40}(OH)_8$ between 16 and 375 K and their standard entropies at 298.15 K, *J. Res. U.S. Geol. Surv., 4,* 631–644, 1976.

Robie, R. A., B. S. Hemingway, and J. R. Fisher, Thermodynamic properties of minerals and related substances at 298.15 K, and 1 bar (10^5 pascals) pressure and at higher temperatures, *U.S. Geol. Surv. Bull., 1452,* 456 pp., 1978.

Ryzhova, T. V., L. M. Reschikova, and K. S. Alexandrov, Elastic properties of rock-forming minerals, VI, Garnets, *Izv. Acad. Sci. USSR Phys. Solid Earth,* Engl. Transl., *7,* 57–64, 1966.

Saxena, S. K., Entropy estimates for some silicates at 298 K from molar volumes, *Science, 193,* 1241–1242, 1976.

Shankland, T. J., and D. H. Chung, General relationships among sound speeds, *Phys. Earth Planet. Interiors, 8,* 121–129, 1974.

Simmons, G., Velocity of compressional waves in various minerals at pressures to 10 kbar, *J. Geophys. Res., 69,* 117, 1964*a*.

Simmons, G., Velocity of shear waves in rocks to 10 kbar, *J. Geophys. Res., 69,* 1123, 1964*b*.

Simmons, G., and H. Wang, *Single Crystal Elastic Constants and Calculated Aggregate Properties: A Handbook,* 2nd ed., 370 pp., MIT Press, Cambridge, Mass., 1971.

Simon, F., and W. Zeidler, Untersuchungen über die spezifischen Wärmen bei tiefen Temperaturen, *Z. Phys. Chem., 123,* 383, 1926.

Skinner, B. J., Thermal expansion, in *Handbook of Physical Constants, Mem. 97,* edited by S. P. Clark, Jr., pp. 75–96, Geological Society of America, Boulder, Colo., 1966.

Stavely, L. A. K., and R. G. Linford, The heat capacity and entropy of calcite and aragonite and their interpretation, *J. Chem. Thermodyn., 1,* 1–11, 1969.

Tarte, P., Experimental study and interpretation of infrared spectra of silicates and germanates, *Mem. Acad. Roy. Sci. Outre Mer Cl. Sci. Tech. Mem. 8 Brussels, 35,* parts 4*a*, *b*, 1965.

Touloukian, Y. S., and C. Y. Ho, *Thermophysical Properties of Matter, TPRC Data Ser.,* vol. 13, *Thermal Expansion, Nonmetallic Solids* 1800 pp., Plenum, New York, 1977.

Ulbrich, H. H., and D. R. Waldbaum, Structural and other contributions to the third-law entropies of silicates, *Geochim. Cosmochim. Acta, 40,* 1–24, 1976.

Vaughn, M. T., and D. J. Weidner, The relationship of elasticity and crystal structure in andalusite and sillimanite, *Phys. Chem. Miner., 3,* 133–144, 1978.

Vedder, W., Correlations between infrared spectrum and composition of mica, *Amer. Mineral., 49,* 736–768, 1964.

Velde, B., Infrared spectra of synthetic micas in the series muscovite-MgAl celadonite, *Amer. Mineral., 63,* 343, 1978.

Verma, R. K., Elasticity of some high-density crystals, *J. Geophys. Res., 65,* 757, 1960.

Wang, H., and G. Simmons, Elasticity of some mantle crystal structures, *J. Geophys. Res., 79,* 2607–2613, 1974.

Westrum, E. F., Jr., E. J. Essene, and D. Perkins, Thermophysical properties of the garnet, grossularite ($Ca_3Al_2Si_3O_2$), *J. Chem. Thermodyn., 11,* 57–66, 1979.

White, W. B., The carbonate minerals, in *The Infrared Spectra of Minerals, Monogr. 4,* edited by V. C. Farmer, pp. 227–284, Mineralogical Society, London, 1974.

White, W. B., Structural interpretation of lunar and terrestrial minerals by Raman spectroscopy, in *Infrared and Raman Spectroscopy of Lunar and Terrestrial Minerals,* edited by C. Karr, Jr., pp. 325–358, Academic, New York, 1975.

Winter, J. K., S. Ghose, and F. P. Okamura, A high-temperature study of the thermal expansion and the anisotropy of the sodium atom in low albite, *Amer. Mineral., 62,* 921–931, 1977.

Woeber, A. F., S. Katz, and T. J. Ahrens, Elasticity of selected rocks and minerals, *Geophysics, 28,* 658–663, 1963.

Wyckoff, R. W. G., *Crystal Structures,* 2nd ed., vol. 4, 566 pp., Interscience, New York, 1968.

Zen, E., Gibbs free energy, enthalpy, and entropy of the rock-forming minerals: Calculations, discrepancies and implications, *Amer. Mineral., 57,* 524–543, 1972.

Ziman, J. M., *Principles of the Theory of Solids,* 2nd ed., 435 pp., Cambridge University Press, New York, 1972.

(Received December 28, 1979;
accepted July 22, 1980.)